



저작자표시-비영리-변경금지 2.0 대한민국

이용자는 아래의 조건을 따르는 경우에 한하여 자유롭게

- 이 저작물을 복제, 배포, 전송, 전시, 공연 및 방송할 수 있습니다.

다음과 같은 조건을 따라야 합니다:



저작자표시. 귀하는 원저작자를 표시하여야 합니다.



비영리. 귀하는 이 저작물을 영리 목적으로 이용할 수 없습니다.



변경금지. 귀하는 이 저작물을 개작, 변형 또는 가공할 수 없습니다.

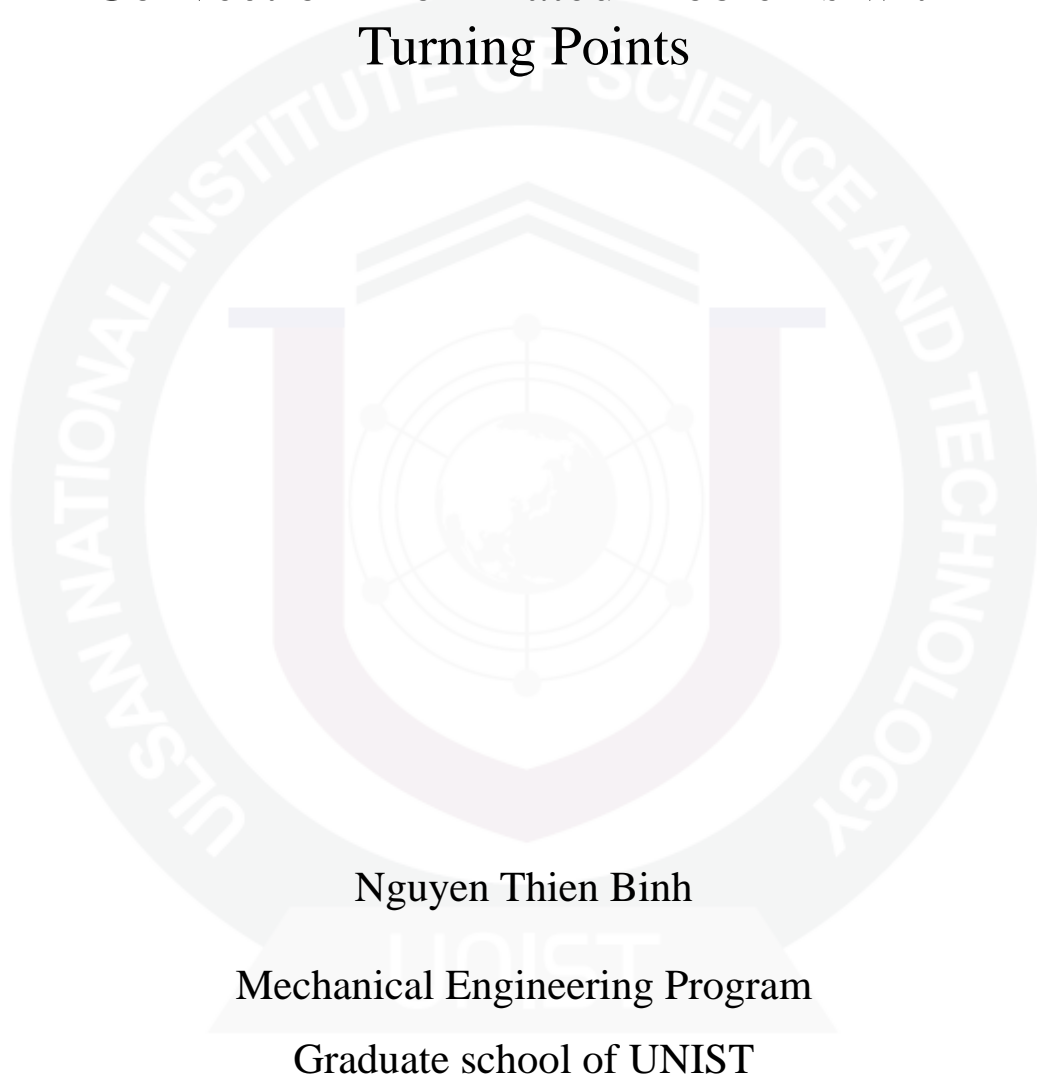
- 귀하는, 이 저작물의 재이용이나 배포의 경우, 이 저작물에 적용된 이용허락조건을 명확하게 나타내어야 합니다.
- 저작권자로부터 별도의 허가를 받으면 이러한 조건들은 적용되지 않습니다.

저작권법에 따른 이용자의 권리는 위의 내용에 의하여 영향을 받지 않습니다.

이것은 [이용허락규약\(Legal Code\)](#)을 이해하기 쉽게 요약한 것입니다.

[Disclaimer](#) 

Semi-Analytical Numerical Methods for Convection-Dominated Problems with Turning Points



Nguyen Thien Binh

Mechanical Engineering Program

Graduate school of UNIST

2012

**Semi-Analytical Numerical Methods for
Convection-Dominated Problems with
Turning Points**

Nguyen Thien Binh

**Mechanical Engineering Program
Graduate School of UNIST**

Semi-Analytical Numerical Methods for Convection-Dominated Problems with Turning Points

A thesis
submitted to the Graduate School of UNIST
in partial fulfillment of the
requirements for the degree of
Master of Science

Nguyen Thien Binh

05.21.2012

Approved by



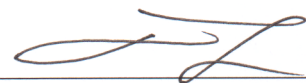
Major Advisor
Chang-Yeol Jung

Semi-Analytical Numerical Methods for Convection-Dominated Problems with Turning Points

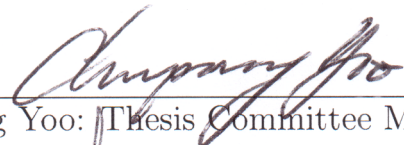
Nguyen Thien Binh

This certifies that the thesis of Nguyen Thien Binh is approved.

05.21.2012



Thesis Supervisor: Chang-Yeol Jung



Chun Sang Yoo: Thesis Committee Member #1



Pilwon Kim: Thesis Committee Member #2

Abstract

In this thesis, we aim to study finite volume approximations which approximate the solutions of convection-dominated problems possessing the so-called interior transition layers. The stiffness of such problems is due to a small parameter multiplied to the highest order derivative which introduces various transition layers at the boundaries and at the interior points where certain compatibility conditions do not meet. Here, we are interested in resolving interior transition layers at turning points. Depending on the characteristics, the latter are identified as turning point layers or characteristic interior layers. The proposed semi-analytic method features interior layer correctors which are obtained from singular perturbation analysis near the turning points. We demonstrate this method is efficient, stable and is of 2^{nd} -order convergence in the approximations.

Contents

List of Figures	vii
List of Tables	viii
I Introduction	1
1.1 Model Introduction	1
1.2 Challenges, Analytic and Numerical Approaches	4
1.3 Objectives	8
II Singular Perturbation Analysis	9
2.1 Regular vs. Singular Perturbations	9
2.2 Singular Perturbation Analysis	15
2.2.1 Case I: f, b compatible	16
2.2.2 Case II: f and b are non-compatible	20
2.3 Apply to our problem	21
III New Numerical Method	24
3.1 Classical Finite Volume	25
3.2 New Finite Volume	28
3.2.1 Compatible Case	28
3.2.2 Noncompatible Case	31
IV Results and Discussions	34
4.1 Compatible Case	34
4.2 Non-compatible Case	35
V Conclusion	41
References	43

List of Figures

Figure 1-1	Solution of Eq. (1.1.2) with $\epsilon = 10^{-1}$ solid curve, and $\epsilon = 10^{-2}$ dashed curve . . .	4
Figure 1-2	Solution of Eq. (1.1.4) with $\epsilon = 10^{-1}$ solid curve, and $\epsilon = 10^{-2}$ dashed curve . . .	5
Figure 3-1	Grid system used for the numerical method.	25
Figure 4-1	(a) Numerical solutions u_N of Eq. (4.1.1) from the classical FVM (cFVM) vs. new FVM (nFVM) using corrector θ^0 : $\epsilon = 10^{-4}$, $N = 40$; (b) Zooming near the transition layer.	36
Figure 4-2	Error plotting of numerical solutions of Eq. (4.1.1) from the cFVM vs. nFVM: $\epsilon = 10^{-4}$, $N = 2^n \times 10$ is the number of control volumes.	37
Figure 4-3	L^2 error plotting of numerical solutions of Eq. (4.1.1) from the nFVM with different values of ϵ , $N = 2^n \times 10$ is the number of control volumes.	37
Figure 4-4	L^∞ error plotting of numerical solutions of Eq. (4.1.1) from the nFVM with different values of ϵ , $N = 2^n \times 10$ is the number of control volumes.	38
Figure 4-5	(a) Numerical solutions u_N from nFVM with $b(x) = x$ and $f(x) = f_j(x)$ for the compatible case: $f_1(x) = x$, $f_2(x) = -\frac{\pi}{2} \operatorname{erf}\left(\frac{1}{\sqrt{2\epsilon}}\right) \left[\frac{\pi}{2}\epsilon \sin\left(\frac{\pi}{2}x\right) - x \cos\left(\frac{\pi}{2}x\right)\right]$, $f_3(x) = xe^x$, $\epsilon = 10^{-4}$, $N = 40$; (b) Zooming near the transition layer.	38
Figure 4-6	(a) Numerical solutions u_N of Eq. (4.2.1) from the cFVM vs. nFVM using two correctors θ^0 and φ^0 : $\epsilon = 10^{-4}$, $N = 40$ for the noncompatible case; (b) Zooming near the transition layer.	39
Figure 4-7	(a) Numerical solutions u_N from nFVM with $b(x) = x$ and $f(x) = f_j(x)$ for the noncompatible case: $f_1(x) = 1$, $f_2(x) = x^3 + 1$, $f_3(x) = e^x$, $\epsilon = 10^{-4}$, $N = 40$; (b) Zooming near the transition layer.	39
Figure 4-8	(a) Numerical solutions u_N from cFVM vs. nFVM with $b(x) = \sin x$, $f(x) = x$, $\epsilon = 10^{-4}$, $N = 40$ for the compatible case; (b) Zooming near the transition layer.	40
Figure 4-9	(a) Numerical solutions u_N from cFVM vs. nFVM with $b(x) = \sin x$, $f(x) = 1$, $\epsilon = 10^{-4}$, $N = 40$ for the noncompatible case; (b) Zooming near the transition layer.	40

List of Tables

Table 3-1	Comparison on L^2 and L^∞ errors of the classical FVM (cFVM) and the new FVM (nFVM) using the corrector θ^0 with the exact solution (4.1.2) of Eq. (4.1.1) with different values of ϵ and numbers of control volumes N	32
Table 3-2	Comparison on L^2 and L^∞ errors of the cFVM and the nFVM with the exact solution (4.1.2) of Eq. (4.1.1), $N = 160$	33

I

Introduction

1.1 Model Introduction

Consider the equation:

$$\begin{cases} L_\epsilon := -\epsilon u_{xx} - bu_x = f & \text{in } \Omega = (-1, 1), \\ u(-1) = u(1) = 0, \end{cases} \quad (1.1.1)$$

where $0 < \epsilon \ll 1$, $b = b(x)$, $f = f(x)$ are smooth on $[-1, 1]$, and for $\delta > 0$, $b < 0$, for $-\delta < x < 0$, $b(0) = 0$, $b > 0$ for $0 < x < \delta$, and $b_x(0) > 0$.

Eq. (1.1.1), in spite of quite simple, contains many interesting and challenging aspects that are worth conducting researches on it. The equation can be seen as a linearized version of a steady convection-diffusion equation. It is well-known that convection-diffusion equations play important roles in many fields of science. They govern natural phenomena which are driven by the interaction of two processes: convection and diffusion. One typical example of these equations is the Navier-Stokes equations which govern the motion of fluid in fluid dynamics. Therefore, understanding the properties of these equations is essential for researchers. In mathematical view, a convection-diffusion equation can be classified into both a parabolic and hyperbolic partial differential equation. In steady state, it takes the form of an elliptic equation. Hence, a full-scale convection-diffusion equation is complicated and thus difficult to conduct an analysis. Let us consider one case for example. Suppose that one wants to develop a new numerical method to approximate the solution of a convection-diffusion equation, one needs first to attack a simpler version of it. For this purpose, Eq. (1.1.1) is a good candidate because it preserves most of important characteristics of a steady convection-diffusion equation that the analyst is aiming for. The second derivative of Eq. (1.1.1) represents the diffusion process with its coefficient ϵ ; whereas the convection or advection process depends on the first derivative. On different circumstances, ϵ is called a viscosity or diffusivity coefficient, and $b(x)u_x$ is a linearized form of the convective acceleration term $\mathbf{u} \cdot \nabla \mathbf{u}$.

In addition, as in our assumption, the diffusivity coefficient ϵ is a very small positive number. This makes the problem (1.1.1) stiff. A stiff problem implies several arguments. Firstly, the behavior of the solution is different in different regions of the problem domain. There exist thin regions in which the solution changes its values rapidly; whereas in other regions, the solution is slowly changing. In a viewpoint of singular perturbation analysis, we name these stiff regions as *layers* or *inner solutions*, and the others are *outer solutions*. Locations of these layers can be at the boundaries or at some points in the interior domain. If a layer displays near a boundary, it is called a *boundary layer*; in the other case, *transition layer* or *interior layer*. The point where an interior transition layer appears is named a *turning point*. And the problem (1.1.1) is called a *boundary layer problem* or *problem having a turning point* depending on which type of layers appearing in the solution. It is noted that the thickness of these layers is very thin and dependent on the parameter ϵ . The second argument we want to refer to a stiff problem is that convection is the dominant process over the diffusion. Convection plays roles almost everywhere of the domain, except at the layers. Inside these layers, diffusion takes place. It helps smooth out the discrepancies between the outer solutions. This explains why we cannot ignore the diffusion term although it is very small in magnitude compared with that of the convection term. One clear example to clarify this is the comparison of the Euler and Navier-Stokes equations. It is known that the former is a viscous-free form of the latter. It is also well-known that discontinuities or shocks may appear in the solutions of the Euler equations even though smooth initial conditions are assumed. But this is not for the Navier-Stokes equations (see [26]). The reason that shocks happening in Euler's solutions is because a viscous term is ignored. Or in viewing of Eq. (1.1.1), it is the removal of the diffusion term.

Physically, boundary and transition layers happen in fluid mechanics. A boundary layer is a thin region at the boundary where the viscous forces dominate other non-viscous ones. On the other hand, transition layers interpret significant physical phenomena, for instance, turbulent boundary layers occurring at the points where the turbulent boundary layer separates since the tangential velocity vanishes and changes sign at such points (see [2]) in fluid dynamics; or the propagation of light in a nonhomogeneous medium as an application of Maxwell's equations in Electromagnetism (see [1]).

We now turn our attention to the convection coefficient $b(x)$. The small parameter ϵ makes the problem stiff and layers occur in the solution; whereas the positions and numbers of these layers are dependent on $b(x)$ and the boundary conditions. We recall that for a convection-diffusion equation of type (1.1.1), convection is the main process and happens in most of the domain. It is well-known that the motion of the quantity u is due to convection, or more precisely, the characteristics of the problem. And the direction of these characteristics depend on the sign of $b(x)$. For our problem (1.1.1), since the convective coefficient $b(x)$ has single zero at $x = 0$, an interior layer displays near the turning point $x = 0$. We consider the following examples to serve as illustrations for boundary layer and interior layer problems.

Example 1.1.1. We solve Eq. (1.1.1) with $b(x) = 1$ and $f(x) = 1$, i.e.,

$$\begin{cases} -\epsilon u_{xx} - u_x = 1 & \text{in } (0, 1), \\ u(0) = u(1) = 0, \end{cases} \quad (1.1.2)$$

for an exact solution as:

$$u = \frac{e^{-\frac{x}{\epsilon}} - 1}{e^{-\frac{1}{\epsilon}} - 1} - x \quad (1.1.3)$$

Example 1.1.2. We now change the convective coefficient $b(x)$ to a function of x , say $b(x) = x$ and let $f(x) = 0$ to have:

$$\begin{cases} -\epsilon u_{xx} - xu_x = 0 & \text{in } (-1, 1), \\ u(-1) = 1, u(1) = -1, \end{cases} \quad (1.1.4)$$

for which an exact solution is available:

$$u \approx \operatorname{erf}\left(-\frac{x}{\sqrt{2\epsilon}}\right), \quad (1.1.5)$$

where,

$$\operatorname{erf}(z) = \frac{2}{\sqrt{\pi}} \int_0^z e^{-s^2} ds. \quad (1.1.6)$$

Solutions of Eqs. (1.1.2)–(1.1.4) are shown in Figs. 1-1–1-2, respectively, for $\epsilon = 10^{-1}, 10^{-2}$. From the figures, we can clearly see slow outer solutions and a stiff boundary at $x = 0$ for the first case, or an interior layer at turning point $x = 0$ for the latter case. The thickness of these layers depends on ϵ . The smaller ϵ is, the stiffer the layers are. And discontinuities do not appear in these cases due to the presence of the layers where diffusion effects take place. In case of boundary layer, i.e. in example 1, the convective coefficient $b(x) = -1 = \text{constant}$. This implies that the characteristics of the problem are $x'(t) = -1$, which causes the boundary layer to occur at the left boundary in order to resolve the condition at this boundary. We therefore cannot ignore the small diffusion term, or else the left boundary is not satisfied. In case $u(0) = 1$ coincidentally, we do can ignore the term, but it is not likely the case to happen physically. For the interior layer case, the characteristics are $x'(t) = -b(x(t)) = -x$ and hence $x' > 0$ for $x \in (-1, 0)$, $x' < 0$ for $x \in (0, 1)$. We thus observe that the characteristics converge to the point $x = 0$. Hence, there is a discontinuity of the outer solutions at the point $x = 0$. In this example, the outer solutions are simply constants. Thus a transition layer is needed to resolve

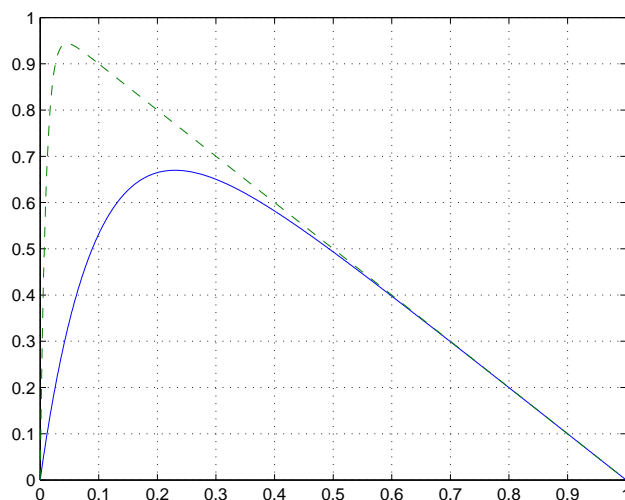


Figure 1-1: Solution of Eq. (1.1.2) with $\epsilon = 10^{-1}$ solid curve, and $\epsilon = 10^{-2}$ dashed curve

the singularity at $x = 0$ (see Fig. 1-2). Moreover, a transition layer may also appear due to logarithmic singularity if the forcing term 0 is replaced by $f(x)$ with $f(0) \neq 0$. This is because of the noncompatibility in the data between $b(x)$ and $f(x)$ of the equation. For example, in Eq. (1.1.4), if $f(x) = 1$, the limit problem (when $\epsilon = 0$) reads $-xu_x = 1$, and thus $u = -\ln|x|$ for $|x| > 0$. Here we observe logarithmic singularity at $x = 0$. This issue will be discussed in chapter 2.

We expand the role of $b(x)$ to more complicated cases. If $b(x)$ has more than one zeros, depending on the boundary conditions, whether multiple interior layers or both boundary and interior layers will occur in the problem domain. If $b(x)$ has zero multiplicity, the solution of the interior layer will have a different form compared to that of single zero. We discuss more on this in the conclusion section.

In the next section, we present analytic and numerical approaches and challenges one faces when studying stiff problems of type (1.1.1). From then, we state the objectives of our work.

1.2 Challenges, Analytic and Numerical Approaches

With the occurrence of the perturbed parameter ϵ in the diffusion term, it is well-known that such problems of the type as in (1.1.1) are stiff problems. Hence, usually, conventional numerical methods using centered discretizations fail in approximating the solutions of these problems. The challenge is that such a good method must give satisfactory approximations for the exponentially thin layers. This difficulty has motivated many researchers to devote their efforts on the problem, both analytically and numerically. In this section, we briefly present difficulties when solving for the solutions of Eq. (1.1.1) and analytic and numerical approaches to it.

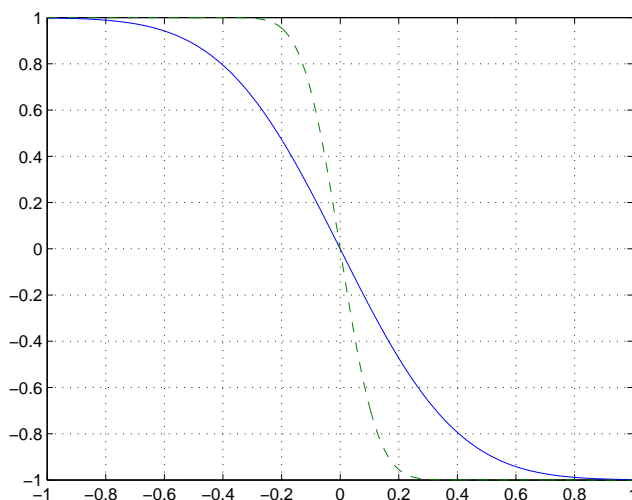


Figure 1-2: Solution of Eq. (1.1.4) with $\epsilon = 10^{-1}$ solid curve, and $\epsilon = 10^{-2}$ dashed curve

A typical analytic approach when studying a stiff convection-diffusion equation is to use so-called singularly perturbation methods. Following these methods, the exact solution is decomposed into outer solutions or outer expansions which approximate the exact solution in the slow-changing regimes; and an inner expansion which is the solution of the boundary or interior layer. These expansions, are then matched to have an analytic approximation of the exact solution. We call this approximation a composite solution. Outer and inner expansions are constructed based on asymptotic expansions. Definition for an asymptotic expansion and how to use it to derive the solutions are presented in chapter 2. Because a composite solution is an analytic approximation of the exact solution, there exists errors between these two. These errors come from the asymptotic expansions in the construction and matching of the solutions, hence are called asymptotic errors. Depending on types of problems to be solved, different perturbation methods are applied. For problems exhibiting boundary layers, typically one uses singularly perturbed methods. Analytic analysis concerns how to construct and match the outer and inner solutions; and more important, to estimate the asymptotic errors of the composite solution. For reference sources, general introduction and classification of perturbation methods can be found in [9], [11]. Singular perturbation methods for ordinary differential equations are presented in [17], and in [27] for nonlinear problems. [7] is a survey of works on the theory of singular perturbations for linear elliptic partial differential equations. Involving the interior layers and turning points, Wasow [23] carefully presents the asymptotic theory for linear equations with turning points. In [5], DeSanti studies the theory for singularly perturbed problems having a turning point with Dirichlet boundary conditions. Recently, in [13], the authors present a full analytic analysis for singularly perturbed convection-diffusion equations exhibiting a turning point. Other researches relating to singular perturbations are addressed in [19], [10], or in [16]

for an analysis of corner singularities, which occur on the corners of the domain boundary in case there are incompatible data. These corners usually induce a local singularity in the solution. If the problem is convective dominant, the corner singularity can be convected into the interior of the domain.

Involving numerical treatments for problem (1.1.1), obstacles for analysts to overcome are two-fold: how they can develop a numerical method which can correctly capture the exponentially thin stiff layer ; yet prevent oscillations from appearing. Difficulties lie in the thin thickness and stiff values of the layer. As indicated, the thickness of this layer depends on the perturbed parameter ϵ , which is often very small in real applications. Hence, in order to capture the rapid transition of the layer, exponentially small grid sizes are needed for the layer, which turns out inefficient or impractical in implementation. In most cases, classical center discretizations do not work because they cannot prevent the non-physical oscillations from happening. We refer readers to section 1, chapter 3 for an explanation of the occurrence of these oscillations in view of mathematical analysis and of practical implementation (see e.g., [18], [22]) Upwind methods, on the other hand, can prevent oscillations but they fail to approximate the layer correctly. In fact, the layer is much smeared out. We use the following example to explain why upwind methods possess the above properties.

Example 1.2.1. Consider we have an equidistant grid system with grid size h and N is the number of grid points, we discretize Eq. (1.1.1) using finite difference method. Supposing that $b(x) \geq \delta > 0$ to have a boundary layer at $x = 0$, we approximate the diffusion and convection term using 2^{nd} -order centered and 1^{st} -order upwind discretizations, respectively, as below:

$$\frac{d^2 u_j}{dx^2} \approx \frac{u_{j+1} - 2u_j + u_{j-1}}{h^2}, \quad \frac{du_j}{dx} \approx \frac{u_j - u_{j+1}}{h}, \quad j = 1, \dots, N-1 \quad (1.2.1)$$

we have Eq. (1.1.1) is discretised:

$$-\epsilon \frac{u_{j+1} - 2u_j + u_{j-1}}{h^2} - b_j \frac{u_j - u_{j+1}}{h} = 0, \quad j = 1, \dots, N-1 \quad (1.2.2)$$

or

$$\left(-\epsilon + \frac{b_j h}{2}\right) \frac{u_{j+1} - 2u_j + u_{j-1}}{h^2} + b_j \frac{u_{j+1} - u_{j-1}}{2h} = 0, \quad j = 1, \dots, N-1. \quad (1.2.3)$$

We note that the convection term can be seen to be approximated by a 2^{nd} -order centered discretization. The coefficient of the diffusion part is now, besides $-\epsilon$, added by additional quantities $\frac{b_j h}{2}$. Because $\epsilon \ll h$ and $b_j = \mathcal{O}(1) > 0$, the former is much less than, and hence, is absorbed by the latter terms. The quantities $\frac{b_j}{2h}$ are called *artificial viscosities* (see e.g., [28]). With the introduction of these artificial viscosities, problem (1.1.1) turns out not stiff anymore.

Hence, it can be approximated without oscillations to occur, but the boundary layer is not as sharp as required, but instead, much smeared out. Indeed, as discussed in [18], by using the discretizations (1.2.1), the order of accuracy of the scheme around the boundary layer is only $\mathcal{O}(1)$, which is absolutely not a desired order. The order in other regions of the problem remains $\mathcal{O}(h)$, which is of the upwind method. We call a numerical method that the order of convergence depends on the location in the domain is *non-uniformly convergent*. The upwind method discussed above is one of this type.

One more drawback of upwind methods we want to address is that it is difficult in implementation for problem (1.1.1) if a turning point is introduced. It is well-known that upwind methods only work if they are designed to follow the characteristics. But in case of problems having turning points, the directions of their characteristics are different in different regions of the problem domains and collide at the turning points causing interior layers to occur. Hence, in order that upwind methods work well for these problems, they have to be equipped with shock-capturing techniques, which are, in general, complicated in developing the algorithms and not uniformly convergent. For the latter attribute, we note that for stability purposes, upwind methods must sacrifice some accuracy near the turning points (see [26]).

There is an observation from the singular perturbation analysis of problem (1.1.1) that different length scales exist in different subdomains of the solution, i.e., the boundary layers and the outer solutions. Hence, for numerical methods, different grid systems are needed in these different regions. This leads to a conclusion that equidistant grid systems are not efficient in this case. Shishkin (see [28]) introduces a *graded mesh* for boundary layer problems. The technique is that grid sizes are more refined when x approaches closer into the layers. It is shown in [18] that schemes based on these graded meshes are uniformly convergent. The matter of how to choose a precise transition point between the coarse mesh and fine mesh for a Shishkin grid has still driven researchers' interests.

An alternative approach to approximate the solution of a convection-dominated problem is to enhance a classical method by incorporating the method with an analytic solution obtained from the analysis via singular perturbation methods. Methods of this approach are called semi-analytical numerical methods. The idea is that the basis spanning the space of numerical solutions of some classical numerical method is embedded with an analytic solution of the layer of Eq. (1.1.1). Then one applies this enriched method to approximate the outer solutions of the problem. By this approach, the layer is captured analytically. Thus the scheme shows uniform convergence on the whole computational domain and the grid system do not need to be adapted following the layer. It much simplifies the scheme and is more efficient compared with the methods using graded grids above. References for this approach include [3], [12], [15]. Reviews of analytic and numerical tools applied for a steady convection-diffusion displaying a boundary layer can be founded in [18], or in [28] for more detailed discussions. Numerical schemes using the enriched techniques for 1D steady convection-diffusion equations having a

boundary layer are studied in [3] in the context of finite element method, in [15] for finite volume method. In [15], the authors develop their scheme to solve a partial differential equation having a boundary layer. For 2D problems, we refer readers to [12] for problems having a parabolic boundary layer, and [14] for convection-diffusion equations in a square domain. For other relating works, see e.g., [24].

1.3 Objectives

In this work, we aim to construct a new numerical method based on enriched techniques developed in [15] and the novel analysis as in [13] for approximating the solution of a stiff convection-diffusion equation having a turning point (1.1.1). We emphasize that our new method is efficient and accurate. The first attribute is due to the usage of an equidistant for discretization purposes on the whole computational domain. Since both the interior layer and the incompatibility in the problem data between $b(x)$ and $f(x)$ are resolved analytically, the new method captures the layer accurately and shows 2^{nd} -order convergence.

We organize our thesis as follows. In chapter 2, we introduce a singular perturbation analysis for the model problem (1.1.1). Based on this, we construct a new numerical method in the context of finite volumes in chapter 3. Numerical results are discussed in chapter 4 to argue for the advantages of the new method. Finally, we close our work with a conclusion chapter.

II

Singular Perturbation Analysis

In this chapter, we present a novel analysis for problem (1.1.1). In the first part, core concepts of perturbation methods are given. We then briefly present results for analyzing problem (1.1.1) following the materials given in [13]. The purposes of this novel analysis are to show that the solution of the turning point problem (1.1.1) can be analytically approximated by a composite expansion comprising outer solutions and an inner layer with estimated asymptotic errors; and the derivation of an analytic approximation of the inner solution which is later treated as a corrector to the classical finite volume space.

2.1 Regular vs. Singular Perturbations

To begin, we first give a definition for a perturbed problem.

Definition 2.1.1. *A problem is called perturbed if one or some of its parts is multiplied with a small parameter $0 < \epsilon \ll 1$.*

If the problem is an equation, in particular, a differential equation, a small parameter ϵ can accompany with any terms in the equation, including its initial data and boundary conditions. Below are some examples of perturbed problems.

Example 2.1.1.

$$x^2 + \epsilon x - 1 = 0, \tag{2.1.1}$$

$$\epsilon x^2 + x - 1 = 0, \tag{2.1.2}$$

$$u_t + u - \epsilon u^2 = 0, \quad u(0) = 1, \tag{2.1.3}$$

$$-\epsilon u_{xx} - u_x = 1, \quad u(0) = u(1) = 0. \tag{2.1.4}$$

For a perturbed problem, we are particularly interested in the behaviors of its solution in its limit, i.e., as $\epsilon \rightarrow 0$. For solving this type of problems, we employ perturbation methods.

The key point is that we construct an asymptotic approximation of the exact solution. An asymptotic approximation is constructed based on the usage of an asymptotic sequence and asymptotic expansion. Before giving definitions for these, we first introduce some notations which are used when we do comparisons between two functions in their limits. These notations are needed for our later construction of an asymptotic expansion.

Suppose we have functions $f(x)$ and $g(x)$ which are formally good enough for our analysis. We write:

$$f(x) = o(g(x)) \quad \text{as } x \rightarrow x_0, \quad (2.1.5)$$

if

$$\lim_{x \rightarrow x_0} \frac{f(x)}{g(x)} = 0, \quad (2.1.6)$$

and we say that “ $f(x)$ is *little-oh* of $g(x)$ ” as $x \rightarrow x_0$.

Similarly, we write:

$$f(x) = \mathcal{O}(g(x)) \quad \text{as } x \rightarrow x_0, \quad (2.1.7)$$

if

$$\lim_{x \rightarrow x_0} \frac{f(x)}{g(x)} = L \neq 1, \quad (2.1.8)$$

and we say that “ $f(x)$ is *big-oh* of $g(x)$ ” as $x \rightarrow x_0$.

Especially, when $L = 1$, we say that “ $f(x)$ and $g(x)$ are *asymptotically equivalent*,” and write:

$$f(x) \sim g(x) \quad \text{as } x \rightarrow x_0. \quad (2.1.9)$$

The above notations give us the information on the behaviors of $f(x)$ and $g(x)$ as $x \rightarrow x_0$. For example, if $f(x)$ is little-oh of $g(x)$ as $x \rightarrow x_0$, it means that $f(x)$ is much smaller than $g(x)$ as $x \rightarrow x_0$ and is negligible when making a comparison between the two. For example, if $f(x) = x^2$ and $g(x) = x$, we say that $f(x) = o(g(x))$ as $x \rightarrow 0$ since it is clear that $f(x) \rightarrow 0$ faster, hence smaller, than $g(x) \rightarrow 0$ as $x \rightarrow 0$. It is noted that the statements above without the part $x \rightarrow x_0$ are meaningless because the notations are used only when the limit case of $f(x)$ and $g(x)$ is considered. In the same manner, $f(x) = \mathcal{O}(g(x))$ as $x \rightarrow x_0$ implies that the two functions are of similar order of x as $x \rightarrow x_0$. Their difference is measured by the limit L . Hence, if $L = 1$, $f(x)$ and $g(x)$ are equivalent, but asymptotically due to $x \rightarrow x_0$. We illustrate the usage of these notations by the following simple examples.

Example 2.1.2. Suppose $f(x) = 2x^2$. We have below statements for different $g(x)$:

- if $g(x) = x$, then $f(x) = o(g(x))$ as $x \rightarrow 0$, but
- $g(x) = o(f(x))$ as $x \rightarrow \infty$.
- if $g(x) = 5x^2 + 6x^3$, then $f(x) = \mathcal{O}(g(x))$ as $x \rightarrow 0$.
- if $g(x) = 2x^2 + 6x^3$, then $f(x) \sim g(x)$ as $x \rightarrow 0$.

We now give a definition for an asymptotic sequence.

Definition 2.1.2. We say a sequence of functions $\{\varphi_n(x)\}_{n=0}^{\infty}$ is an asymptotic sequence if

$$\varphi_{n+1}(x) = o(\varphi_n(x)), \quad \text{as } x \rightarrow x_0 \quad (2.1.10)$$

for every n .

With the above discussions, we finally come with a definition for an asymptotic expansion, following the one given in [11]:

Definition 2.1.3. The series of terms written as

$$\sum_{n=0}^N a_n \varphi_n(x) + \mathcal{O}(\varphi_{N+1}(x)), \quad (2.1.11)$$

where the a_n can be constants or functions which are independent of x , is an asymptotic expansion or asymptotic approximation of $f(x)$, with respect to the asymptotic sequence $\{\varphi_n(x)\}_{n=0}^{\infty}$ if, for every $N \geq 0$

$$f(x) - \sum_{n=0}^N a_n \varphi_n(x) = o(\varphi_N(x)), \quad \text{as } x \rightarrow x_0. \quad (2.1.12)$$

The term $R = o(\varphi_N(x))$ is called an asymptotic error of the approximation. We can also write:

$$f \sim \sum_{n=0}^N a_n \varphi_n(x), \quad \text{as } x \rightarrow x_0. \quad (2.1.13)$$

From the above definition, we notice that given function $f(x)$ and $x \rightarrow x_0$, the asymptotic expansion of $f(x)$ is not unique. In fact, with different asymptotic sequences, we can construct different asymptotic expansions of $f(x)$ if they exist. But if the above condition, i.e., given $f(x)$ and $x \rightarrow x_0$, goes with a predefined asymptotic sequence, the asymptotic expansion of $f(x)$ is then unique since each a_n can be computed analytically (see [11]) as follows:

Consider

$$\frac{f(x) - \sum_{n=0}^{N-1} a_n \varphi_n(x)}{\varphi_N(x)} = \frac{f(x) - \sum_{n=0}^N a_n \varphi_n(x) + a_N \varphi_N(x)}{\varphi_N(x)} \quad (2.1.14)$$

$$= \frac{f(x) - \sum_{n=0}^N a_n \varphi_n(x)}{\varphi_N(x)} + a_N. \quad (2.1.15)$$

Taking the limit, we obtain:

$$a_N = \frac{f(x) - \sum_{n=0}^N a_n \varphi_n(x)}{\varphi_N(x)}. \quad (2.1.16)$$

It is also noted that an asymptotic expansion of $f(x)$ need not to converge to $f(x)$ as $x \rightarrow x_0$. In fact, most of the asymptotic expansions are divergent as $x \rightarrow x_0$ (see the example on p.12, [9] for an illustration). This implies that adding more terms into an asymptotic expansion does not result in a decrease in the asymptotic error. In fact, as we mentioned in the definition of an asymptotic expansion, the terms, e.g., $\varphi_{n+1}(x) = o(\varphi_n(x))$ only when $x \rightarrow x_0$. Hence, if we fix x , we have no conclusion in comparing the magnitudes between $a_{n+1}\varphi_{n+1}(x)$ and $a_n\varphi_n(x)$. In other words, an asymptotic expansion relates to an approximation of f in a limit sense, i.e., fixing n and letting $x \rightarrow x_0$; whereas adding terms relates to fixing x and letting $n \rightarrow \infty$. These two cases are different in general.

We now use asymptotic expansions to analytically approximate the first 2 quadratic equations in example 2.1.1 to illustrate for 2 types of perturbed problems: regularly and singularly. We notice that the asymptotic expansions of the solutions of a perturbed problem are constructed based on asymptotic sequences of the small parameter ϵ , not of the variable x of the problem.

Example 2.1.3.

$$x^2 + \epsilon x - 1 = 0, \quad 0 < \epsilon \ll 1. \quad (2.1.17)$$

We can easily calculate the exact solutions of Eq. (2.1.17):

$$x_{1,2} = \frac{1}{2} \left(-\epsilon \pm \sqrt{\epsilon^2 + 4} \right). \quad (2.1.18)$$

Substituting the asymptotic expansion of x : $x \sim \sum_{j=0}^{\infty} a_j \epsilon^j$ into Eq. (2.1.17), we obtain:

$$\left(\sum_{j=0}^{\infty} a_j \epsilon^j \right)^2 + \epsilon \left(\sum_{j=0}^{\infty} a_j \epsilon^j \right) - 1 = 0. \quad (2.1.19)$$

Balancing terms at each order of ϵ gives us:

$$\left\{ \begin{array}{l} \mathcal{O}(1) : a_0^2 - 1 = 0, \\ \mathcal{O}(\epsilon) : 2a_0a_1 + a_0 = 0, \\ \mathcal{O}(\epsilon^2) : a_1^2 + 2a_1a_2 + a_1 = 0, \\ \dots \end{array} \right. \quad (2.1.20)$$

Solving for a_j , we obtain two expansions which approximate the two zeros of Eq. (2.1.17):

$$x_1 = 1 - \frac{1}{2}\epsilon + \frac{1}{8}\epsilon^2 + \mathcal{O}(\epsilon^3), \quad (2.1.21)$$

and

$$x_1 = -1 - \frac{1}{2}\epsilon - \frac{1}{8}\epsilon^2 + \mathcal{O}(\epsilon^3), \quad (2.1.22)$$

We observe that as $\epsilon \rightarrow 0$, the asymptotic expansions give satisfactory approximations to the exact zeros of the quadratic equation. Furthermore, these approximations also agree with the zeros of the limit case, i.e., $x^2 - 1 = 0$. This implies the occurrence of the small term ϵx in Eq. (2.1.17) plays little roles in the equation, hence it is possible if we neglect this term and consider it is absorbed by other bigger terms. We call a perturbed problem in which ϵ does not effect the behaviors of the solutions of the problem as $\epsilon \rightarrow 0$ a *regularly* perturbed problem.

Example 2.1.4. We now make a small change in Eq. (2.1.17) by shifting ϵ to accompany with the higher-order term, i.e. x^2 , to have:

$$\epsilon x^2 + x - 1 = 0, \quad 0 < \epsilon \ll 1, \quad (2.1.23)$$

for which exact solutions are calculated:

$$x_1 = \frac{-1 + \sqrt{1 + 4\epsilon}}{2\epsilon} \rightarrow 1 \quad \text{as } \epsilon \rightarrow 0, \quad (2.1.24)$$

$$x_2 = \frac{-1 - \sqrt{1 + 4\epsilon}}{2\epsilon} \rightarrow \infty \quad \text{as } \epsilon \rightarrow 0. \quad (2.1.25)$$

Carrying the technique as above with an expansion $x \sim \sum_{j=0}^{\infty} a_j \epsilon^j$, we find that:

$$x_1 = 1 - \epsilon + 2\epsilon^2 + \mathcal{O}(\epsilon^3), \quad (2.1.26)$$

We notice that by applying the same technique of a regularly perturbed problem, we can only

obtain one zero of Eq. (2.1.23). This zero is also the one of its limit case, i.e. $x - 1 = 0$. The other is missing. To seek for the missing zero, we use a technique called singular perturbation.

We proceed as follows:

Set:

$$X = \epsilon x \quad \Rightarrow \quad x = \epsilon^{-1} X \quad (2.1.27)$$

Eq. (2.1.23) is rewritten:

$$\epsilon^{-1} X^2 + \epsilon^{-1} X - 1 = 0 \quad (2.1.28)$$

Substituting the expansion $X = \sum_{n=0}^{\infty} X_n \epsilon^n$ into Eq. (2.1.28), and follow the steps as in the regular case, we obtain:

$$\begin{cases} x_1 = -\frac{1}{\epsilon} - 1 + \epsilon + \dots, \\ x_2 = 1 - \epsilon + \dots \end{cases} \quad (2.1.29)$$

We note that by using a change in the variable x , we retrieve 2 expansions, which give satisfactory approximations to the zeros of the equation. We explain more on why a regularly asymptotic expansion can only capture one zero and miss the other. We note that the behaviors of the two roots are very different as $\epsilon \rightarrow 0$. The root $x = 1$ is the intersection point of the graph of $\epsilon x^2 + x - 1 = 0$ and its limit form $x - 1 = 0$, hence remains unchanged as $\epsilon \rightarrow 0$. The other, which depends strictly on ϵ , goes to $-\infty$ when $\epsilon \rightarrow 0$. Hence, an expansion with a stretched variable is needed in this case.

From the above example, an observation is that although the term ϵx^2 is small compared to the others, it plays an important role. If we ignore the term, the properties of the equation change completely (e.g. from a quadratic to linear equation as in our example). We call such type of problems *singularly* perturbed problems.

Remark 2.1.1. • In case of a differential equation which is of singularly perturbed types, a separation of the solution domain into sub-domains possessing different behaviors and the occurrence of a layer as $\epsilon \rightarrow 0$ is observed. As proceeded in example 2.1.4, we apply singular perturbation methods to handle this case. We use a regularly asymptotic expansion to seek for the outer solutions, and an expansion using a stretched variable to derive the approximation of the layer analytically.

- For our Eq. (2.2.1), the problem is more complicated because not only the interior layer is stiff, but also the outer solutions do if the incompatibility happens between the convection

and force terms (see the condition (2.2.11) below). We refer readers to the discussion of the example 1.1.2. In [13], the authors present a full analysis via singularly perturbation for a problem of type (2.2.1) having a turning point. These results provide us an insight about the behaviors of the solution as $\epsilon \rightarrow 0$ to construct our new numerical method for the problem.

In the next section, to set up the mathematical foundation for our later development of the new method, we briefly summarize important results from [13], and then apply it to our case.

2.2 Singular Perturbation Analysis

In this section, we present a singular perturbation analysis for the problem for which we will construct a new numerical method in the next section. As mentioned in the introduction section, the problem we are dealing with is a steady convection-dominated equation. For the sake of clarification, we rewrite the model as below:

$$\begin{cases} -\epsilon^2 u_{xx} - bu_x = f & \text{in } \Omega = (-1, 1), \\ u(-1) = u(1) = 0, \end{cases} \quad (2.2.1)$$

where $0 < \epsilon \ll 1$, $b = b(x)$, $f = f(x)$ are smooth on $[-1, 1]$, and for $\delta > 0$, $b < 0$, for $-\delta < x < 0$, $b(0) = 0$, $b > 0$ for $0 < x < \delta$, and $b_x(0) > 0$. The ϵ^2 serves for simpler formulae and calculations and to agree with the analysis given in [13].

As stated in the previous section, the convection-diffusion model (2.2.1) is a type of singular perturbed problem, i.e., there exists a thin layer in the domain in which the solution changes rapidly. Because $b(x)$ changes sign at $x = 0$, this transition layer occurs at this turning point.

Via singular perturbation methods, we present how to derive the outer expansions of the solution and the exact solution of the interior layer. Furthermore, we indicate that the asymptotic errors of the composite solution, i.e., the combination of the outer expansions and interior layer to make an approximation of the exact solution, depend on the asymptotic parameter ϵ and get smaller when there are more terms in the expansions are used. Here, we use the word *approximation* to refer to an analytical approximation, not to an approximate solution given by a numerical method.

One of the challenges when dealing with singularly perturbed problems exhibiting an interior layer to those having boundary layers is that, besides the troublesome of the layer analysis, one must also care about the position of the turning point, and the complexity of the outer expansions around this point. For the former, thanks to the linearity of our model, we know exactly that the turning point, hence the interior layer, is located at $x = 0$. And for the later remark, as presented in the introductory example 1.1.2 in the introduction section, if the data between $b(x)$ and $f(x)$ are not compatible, as well as the stiff solution of the interior layer, the

outer expansions also exhibit stiff solutions, e.g., due to logarithmic singularities. To recall, for Eq. (2.2.1), if $f(0) = 1$ on the whole domain, the limit problem (i.e., when $\epsilon = 0$) reads $-u_x = 1$, and thus $u = -\ln|x|$ for $|x| > 0$. Here we observe a logarithmic singularity at $x = 0$. Hence, it is natural to classify the singular perturbation analysis of our problem into two cases dependent on the compatibility condition of $b(x)$ and $f(x)$.

2.2.1 Case I: f, b compatible

We first give a mathematical analysis for the case that f and b are compatible to each other. The procedure is as follows. We seek for the approximations of the outer solutions using regularly asymptotic expansions. For the interior layer, we use a stretched variable to derive the inner solutions or the approximations of the interior layer. We then present the estimates of the asymptotic errors of these expansions and of the composite solution compared to the exact solution.

We now construct the outer expansions for the solutions of Eq. (2.2.1). Via this, we indicate the compatibility condition for f and b .

• *Outer expansions*

Substituting formal expansions:

$$u \sim \sum_{j=0}^{\infty} \epsilon^j u_l^j \quad \text{in } x < 0 \quad (2.2.2)$$

and,

$$u \sim \sum_{j=0}^{\infty} \epsilon^j u_r^j \quad \text{in } x > 0, \quad (2.2.3)$$

into the Eq. (2.2.1), and balancing terms at each $\mathcal{O}(\epsilon)$, we derive:

$$\mathcal{O}(1) : -bu_{lx}^0 = f \quad \text{in } [-1, 0) \quad -bu_{rx}^0 = f \quad \text{in } (0, 1], \quad (2.2.4)$$

$$\mathcal{O}(\epsilon) : -bu_{lx}^1 = 0 \quad \text{in } [-1, 0) \quad -bu_{rx}^1 = 0 \quad \text{in } (0, 1], \quad (2.2.5)$$

$$\mathcal{O}(\epsilon^j) : -bu_{lx}^0 = u_{lxx}^{j-2} \quad \text{in } [-1, 0) \quad -bu_{rx}^0 = u_{rxx}^{j-2} \quad \text{in } (0, 1], \quad (2.2.6)$$

for $j \geq 2$,

with boundary conditions for all equations above to be $u_l^j(-1) = u_r^j(1) = 0, j \geq 0$.

Analytical solutions of Eqs.(2.2.4)–(2.2.6) are available and as follows:

$$u_l^0 = - \int_{-1}^x b(s)^{-1} f(s) ds, \quad u_r^0 = - \int_x^1 b(s)^{-1} f(s) ds, \quad (2.2.7)$$

$$u_l^{2k} = - \int_{-1}^x b(s)^{-1} u_{xx}^{2(k-1)}(s) ds, \quad u_r^{2k} = - \int_x^1 b(s)^{-1} u_{xx}^{2(k-1)}(s) ds, \quad (2.2.8)$$

for all $j = 2k, k \geq 1$,

$$u_l^j = u_r^j = 0, \quad \text{for all odd } j\text{'s}. \quad (2.2.9)$$

From the integrations (2.2.7)–(2.2.8), to make sure the regularities of the outer solutions, i.e.:

$$\left| \frac{d^m u_l^{2k}}{dx^m}(0^-) \right|, \quad \left| \frac{d^m u_r^{2k}}{dx^m}(0^+) \right| \leq \kappa_{km}, \quad (2.2.10)$$

with $m \geq 1$ and $k \geq 0$ and κ is a constant independent of ϵ which depends on k, m , we need the following condition, i.e., the compatibility condition of b and f :

$$\frac{d^i f}{dx^i}(0) = 0, \quad i = 0, 1, \dots, N, \quad (2.2.11)$$

with $N = m + 2k - 1$.

• *Interior layers* $\theta_l^j, \theta_r^j, \zeta^j$

From the condition (2.2.11), we now guarantee that there are no singularities in the outer solutions around $x = 0$ as $\epsilon \rightarrow 0$. But usually, the values $u_l^j(0^-) \neq u_r^j(0^+)$. To resolve these discrepancies between the outer solutions smoothly, we introduce the inner expansions $\sum_{j=0}^{\infty} \epsilon^j \theta_l^j, \sum_{j=0}^{\infty} \epsilon^j \theta_r^j$ with $\theta_l^j = \theta_l^j(\bar{x}), \theta_r^j = \theta_r^j(\bar{x})$ where $\bar{x} = x/\epsilon$ is called a stretched variable. Substituting these expansions into Eq. (2.2.1), and the formal Taylor expansion for $b = b(x)$ at $x = 0$:

$$b(x) = \sum_{j=1}^{\infty} b_j x^j = \sum_{j=1}^{\infty} b_j \epsilon^j \bar{x}^j, \quad (2.2.12)$$

where $b_j = \frac{1}{j!} \frac{d^j b}{dx^j}(0)$; we note that here j starts from 1 due to $b_0 = b(0) = 0$; we have Eq. (2.2.1) written as below:

for $x \in (-\infty, 0)$:

$$\left\{ \begin{array}{l} -\left(\sum_{j=0}^{\infty} \epsilon^j \theta_{l\bar{x}\bar{x}}^j\right) - \left(\sum_{j=1}^{\infty} b_j \epsilon^{j-1} \bar{x}^j\right) \left(\sum_{j=0}^{\infty} \epsilon^j \theta_{l\bar{x}}^j\right) = 0, \\ \sum_{j=0}^{\infty} \epsilon^j \theta_l^j(\bar{x}) = u_r(0^+), \\ \sum_{j=0}^{\infty} \epsilon^j \theta_{l\bar{x}}^j(\bar{x}) = \sum_{j=0}^{\infty} \epsilon^{j+1} \theta_{lx}^j = u_{rx}(0^+) \quad \text{at } \bar{x} = 0; \end{array} \right. \quad (2.2.13)$$

for $x \in (0, \infty)$:

$$\left\{ \begin{array}{l} -\left(\sum_{j=0}^{\infty} \epsilon^j \theta_{r\bar{x}\bar{x}}^j\right) - \left(\sum_{j=1}^{\infty} b_j \epsilon^{j-1} \bar{x}^j\right) \left(\sum_{j=0}^{\infty} \epsilon^j \theta_{r\bar{x}}^j\right) = 0, \\ \sum_{j=0}^{\infty} \epsilon^j \theta_r^j(\bar{x}) = u_l(0^-), \\ \sum_{j=0}^{\infty} \epsilon^j \theta_{r\bar{x}}^j(\bar{x}) = \sum_{j=0}^{\infty} \epsilon^{j+1} \theta_{rx}^j = u_{lx}(0^-) \quad \text{at } \bar{x} = 0. \end{array} \right. \quad (2.2.14)$$

Again, balancing terms at each $\mathcal{O}(\epsilon)$, we obtain the equations for each θ_r^j :

$$\mathcal{O}(1) : \left\{ \begin{array}{l} -\theta_{r\bar{x}\bar{x}}^0 - b_1 \bar{x} \theta_{r\bar{x}}^0 = 0, \\ \theta_r^0(\bar{x}) = u_l^0(0^-), \quad \theta_{r\bar{x}}^0(\bar{x}) = \epsilon u_l^0(0^-) \quad \text{at } \bar{x} = 0, \end{array} \right. \quad (2.2.15)$$

$$\mathcal{O}(\epsilon) : \left\{ \begin{array}{l} -\theta_{r\bar{x}\bar{x}}^1 - b_1 \bar{x} \theta_{r\bar{x}}^1 = b_2 \bar{x}^2 \theta_{r\bar{x}}^0, \\ \theta_r^1(\bar{x}) = u_l^1(0^-), \quad \theta_{r\bar{x}}^1(\bar{x}) = \epsilon u_l^1(0^-) \quad \text{at } \bar{x} = 0, \end{array} \right. \quad (2.2.16)$$

$$\mathcal{O}(\epsilon^j) : \left\{ \begin{array}{l} -\theta_{r\bar{x}\bar{x}}^j - b_1 \bar{x} \theta_{r\bar{x}}^j = \sum_{k=0}^{j-1} b_{j-k+1} \bar{x}^{j-k+1} \theta_{r\bar{x}}^k, \\ \theta_r^j(\bar{x}) = u_l^j(0^-), \quad \theta_{r\bar{x}}^j(\bar{x}) = \epsilon u_l^j(0^-) \quad \text{at } \bar{x} = 0, \end{array} \right. \quad (2.2.17)$$

which allow us to determine θ_r^j explicitly. Notice that $u_r^j = u_l^j = 0$ for j odd. In particular, for $j = 0, 1$, we find that:

$$\theta_r^0 = \epsilon u_{lx}^0(0^-) \int_0^{\bar{x}} \exp\left(-\frac{b_1 s^2}{2}\right) ds + u_j^0(0^-), \quad (2.2.18)$$

$$\theta_r^1 = -\epsilon u_{lx}^0(0^-) b_2 3^{-1} \int_0^{\bar{x}} s^3 \exp\left(-\frac{b_1 s^2}{2}\right) ds + u_j^0(0^-). \quad (2.2.19)$$

Here, we note that as $\bar{x} \rightarrow \infty$,

$$\theta_r^0 \rightarrow \epsilon u_{lx}^0(0^-) c_{r,0} + u_l^0(0^-) =: c_{r,\infty}^0(\epsilon), \quad (2.2.20)$$

$$\theta_r^1 \rightarrow -\epsilon u_{lx}^0(0^-) b_2 3^{-1} c_{r,1} =: c_{r,\infty}^1(\epsilon), \quad (2.2.21)$$

where $c_{r,0} = \int_0^\infty \exp(-b_1 s^2/2) ds$, $c_{r,1} = \int_0^\infty s^3 \exp(-b_1 s^2/2) ds$.

Remark 2.2.1. 1. Solutions of θ_l^j can be deduced in a similar procedure.

2. The source term f only affects the outer expansions, thus it does not appear in Eqs. (2.2.13)–(2.2.14).
3. We explain more on the boundary conditions used in Eq. (2.2.13) and (2.2.14). The Dirichlet boundary conditions are to make sure continuity of the outer and inner solutions at the matching points; whereas the smoothness of the approximation at these joints are guaranteed by the Neumann boundary conditions.

We are now close to a composite expansion which asymptotically approximates solution u of Eq. (2.2.1). We denote the functions $g^j := -(u_l^j \cup \theta_r^j) - (\theta_l^j \cup u_r^j)$ where the notation $\phi \cup \varphi$ is for a function on $(-1, 1)$ equal to (the restriction of) ϕ on $(-1, 0)$ and to (the restriction of) φ on $(0, 1)$. We notice that, by (2.2.20), u and g^j are different from each other quantities $-c_{l,\infty}^j$ at $x = -1$ and $-c_{r,\infty}^j$ at $x = 1$. To remedy these discrepancies, we introduce more interior layers ζ^j which are same as θ_l^j and θ_r^j , i.e., ζ^j are also derived from Eqs. (2.2.15)–(2.2.17), but have different boundary conditions:

$$\zeta^j = -\theta_l^j \quad \text{at } x = -1, \quad \zeta^j = -\theta_r^j \quad \text{at } x = 1 \quad \text{for } j \geq 0. \quad (2.2.22)$$

With the introduction of ζ , we define a composite expansion:

$$\tilde{g}_{\epsilon n} := \psi_{\epsilon n} + \eta_{\epsilon n} + \zeta_{\epsilon n} \sim u, \quad (2.2.23)$$

where

$$\psi_{\epsilon n} = \sum_{j=0}^{2n} \epsilon^j (u_l^j \cup \theta_r^j), \quad \eta_{\epsilon n} = \sum_{j=0}^{2n} \epsilon^j (\theta_l^j \cup u_r^j), \quad \zeta_{\epsilon n} = \sum_{j=0}^{2n} \epsilon^j \zeta^j. \quad (2.2.24)$$

In [13], we have the following estimate for the asymptotic errors of the expansion (2.2.23):

$$\|u - \tilde{g}_{\epsilon n}\|_{H^m(\Omega)} \leq \kappa_n \epsilon^{2n+3/2} \phi(\epsilon, m), \quad m = 0, 1, 2, \quad (2.2.25)$$

where $\phi(\epsilon, m)$ is defined:

$$\phi(\epsilon, m) = \begin{cases} 1 & \text{for } m = 0, \\ \epsilon^{-1} & \text{for } m = 1, \\ \epsilon^{-3} & \text{for } m = 2. \end{cases} \quad (2.2.26)$$

Remark 2.2.2. 1. From (2.2.25), we observe that the asymptotic errors become smaller when more terms in the composite expansion (2.2.23) are introduced.

2. From the error estimation (2.2.25), we notice that the solution of Eq. (2.2.1) can be

approximated by the composite expansion (2.2.23) using singular perturbation methods. Moreover, from this expansion, it is shown that the solution can be decomposed into a slow part which represents for the slow outer solutions, and a fast part which is the stiff interior layer.

3. In the above analysis, three types of interior layers, i.e., θ_l^j , θ_r^j , and ζ^j , are used for the matching purpose, which are different from a conventional matched asymptotic technique. We recall that for the latter, only one approximation for the interior layer is sought for by solving equation (2.2.13) or (2.2.14) without injecting boundary conditions. Hence, there are two integration constants remained. These constants are then verified through a matching process of the inner and outer solutions. This matching is carried out in transition regions where both inner and outer solutions approach to the same values. Hence, there exist two common terms in the composite expansion, in which one is needed to be subtracted (see [11]). For the analysis presented in this work, via the applying of the boundary conditions when solving for interior layers θ_l^j , θ_r^j as in Eqs. (2.2.13) and (2.2.14), the discrepancies of the outer solutions are moved to two boundaries, and then resolved by other layers, i.e., ζ^j by fulfilling the boundary conditions of Eq. (2.2.1). Hence, no common terms result in our composite expansion (2.2.23).
4. The above remarks provide us the idea of constructing a numerical method for approximating u . The procedure is that we first seek for an analytical approximation of the interior layer via singular perturbations (as presented in this section); then we numerically approximate the outer solutions by a type of numerical methods. In this thesis, we use finite volume method. Unlike the analytical analysis to use three interior layers serving for the matching of the inner and outer solutions, in our numerical methods, we remedy these discrepancies numerically via redefining the boundary conditions satisfying the problem (2.2.1). This method will be presented in the next chapter.

2.2.2 Case II: f and b are non-compatible

In this section, we briefly present the case that f and b are non-compatible, that is, the condition (2.2.11) is violated. As presented in example 2 in the introduction, for this case, the solution is stiff not only in the interior layer but also in the outer solutions near the turning point. This is due to logarithmic singularities due to the incompatibility of b and f .

As proven in [13], one can still apply the analysis for case I above given that f is decomposed

into \hat{f} and B_j as below:

$$\hat{f} = f - \sum_{k=0}^N \gamma_k B_k(x), \quad (2.2.27)$$

where

$$B_0 = b_x(x), \quad B_1 = b(x), \quad B_{k+2} = b(x) \int_0^x B_k(s) ds, \quad k \geq 0. \quad (2.2.28)$$

We note that since $\frac{d^i B_k}{dx^i}(0) = 0$ for $i < k$ and $\frac{d^i B_k}{dx^i}(0) \neq 0$ for $i = k$, we can recursively find that all the γ_k , $k \geq 0$ so that the compatibility condition (2.2.11) holds for \hat{f} . For the other terms, i.e., $\sum_{k=0}^N \gamma_k B_k(x)$, it turns out that singularities happen only for terms B_k , $k = 2J$, $J \geq 0$.

The analysis procedure of the interior layers in this case is similar to that in the previous section. The only change is that due to singularities at $x = 0$, we do not match the solutions at $x = 0$ but rather at the boundaries $x = -1$ and $x = 1$, For detailed arguments, see [13].

2.3 Apply to our problem

From the analysis above, in case of a compatible f , we notice that the solution u of Eq. (1.1.1) can be decomposed into a stiff part (the transition layer), where large values of the derivative are observed, and the non-stiff part (outer solutions) away from the turning point. We, therefore, introduce a decomposition of the solution u as follows:

$$u = u_s + \lambda \theta^0, \quad (2.3.1)$$

where u_s is considered a slow variable, θ^0 is the transition layer defined by (2.3.6) below, and λ an unknown.

We now derive the interior layer. We recall that for our problem, the turning point is $x_0 = 0$. We first start with a compatible f , i.e., $f(x_0) = 0 = b(x_0)$. In this case, the outer expansions are considered slow. Using a formal asymptotic expansion for the solution u at the transition layer, and Taylor expansion for b about $x = x_0 = 0$, we write:

$$u \sim \sum_{k=0}^{\infty} \epsilon^k \theta^k(\bar{x}), \quad \bar{x} = \frac{x - x_0}{\sqrt{\epsilon}}. \quad (2.3.2)$$

and

$$b \sim \sum_{k=0}^{\infty} \frac{1}{k!} b_k (\sqrt{\epsilon})^k \bar{x}^k, \quad (2.3.3)$$

where b_k are k^{th} order derivatives of b with respect to x , at $x = 0$. Substituting these expansions into Eq. (1.1.1) with a note that $b(0) = f(0) = 0$, and balancing terms, we can obtain a system of equations at each order of ϵ . It turns out that, for numerical purposes, the leading term θ^0 suffices to catch the sharp transition layer, which is the solution of

$$-\theta_{\bar{x}\bar{x}}^0 - b_1 \bar{x} \theta_{\bar{x}}^0 = 0; \quad (2.3.4)$$

this equation is the zeroth order approximation near $x = 0$ of

$$-\epsilon \theta_{xx} - b(x) \theta_x = 0. \quad (2.3.5)$$

Transforming Eq. (2.3.4) back to variable x , we obtain

$$-\epsilon \theta_{xx}^0 - b_1 x \theta_x^0 = 0; \quad (2.3.6)$$

whose an explicit form of θ^0 is available:

$$\theta^0 = \frac{2}{\sqrt{\pi}} \int_0^{x\sqrt{\frac{b_1}{2\epsilon}}} e^{-s^2} ds = erf\left(x\sqrt{\frac{b_1}{2\epsilon}}\right). \quad (2.3.7)$$

The corrector θ^0 will be incorporated into the classical finite volume space V_h to absorb transition layer singularity (see section 2.3). We can infer from the local asymptotic behavior (2.3.7) that exponentially refined meshes are required at $x = 0$ for the classical numerical method. This leads to expensive computations, even more expensive in higher dimensional problems.

In the case of a noncompatible f , i.e., $f(0) \neq 0 = b(0)$, as well as the inner expansion, the outer expansions also display sharp transitions like spikes, e.g., logarithm, due to the small variable $b(x)$ and non-degenerate $f(x)$ near $x = 0$. In order to resolve the sharp transition due to the noncompatibility between $b(x)$ and $f(x)$ at $x = 0$, we introduce the zeroth corrector φ^0 :

$$\varphi^0 = - \int_0^{\frac{x}{\sqrt{\epsilon}}} \int_0^t \exp\left(-b_1 \frac{t^2 - s^2}{2}\right) ds dt. \quad (2.3.8)$$

The φ^0 is the solution of the equation:

$$-\epsilon \varphi_{xx}^0 - b_1 x \varphi_x^0 = 1, \quad (2.3.9)$$

which is the zeroth order approximation near $x = 0$ of

$$-\epsilon \varphi_{xx} - b(x) \varphi_x = 1. \quad (2.3.10)$$

Using polar coordinates $s = r \cos \theta$, $t = r \sin \theta$ in (2.3.8), we rewrite $\varphi^0(x)$:

$$\varphi^0(x) = -\frac{1}{b_1} \int_{\frac{\pi}{4}}^{\frac{\pi}{2}} \frac{1}{\cos 2\theta} \left[\exp\left(\frac{b_1 \cos 2\theta x^2}{2 \sin^2 \theta \epsilon}\right) - 1 \right] d\theta. \quad (2.3.11)$$

Notice that the double integration (2.3.8) is transformed to the single one (2.3.11). Hence, computational cost in the numerical simulations will be much reduced.

Substituting (2.3.1) into Eq. (3.1.1) and using (2.3.5), we can write:

$$L_\epsilon(u_s + \lambda(\theta^0 - \theta)) = f(x), \text{ in } \Omega, \quad (2.3.12)$$

which is supplemented with boundary conditions:

$$\begin{cases} u_s(-1) + \lambda\theta^0(-1) = u(-1) = 0, \\ u_s(1) + \lambda\theta^0(1) = u(1) = 0. \end{cases} \quad (2.3.13)$$

The slow variable u_s will be approximated by the usual step functions and we now propose a new finite volume method in the following chapter.

III

New Numerical Method

In this chapter, we present a new numerical method for problem (1.1.1) based on a classical finite volume method and the novel analysis given in the previous chapter. The chapter is divided into two parts. In the first part, we apply classical Finite Volume methods to solve for an approximate solution of the problem (1.1.1) numerically. The purposes for this part are two-fold: to introduce numerical concepts from the numerical method that are used in our specific cases; and to explain why such a classical method fails for approximating a stiff problem. Then, in the second part, we incorporate the analytic approximation (2.3.7) into the classical method to produce a new and accurate method.

Finite volume methods approximate the solution of a differential equation by its integral form. The computational domain is divided into a finite number of small intervals called control volumes. One then approximates the solution at each control volume by its average value on that control volume via the fluxes coming in and out the volume through its edges (see [22], [25]). Finite volume methods have advantages compared with other numerical methods. Firstly, the average values of the control volumes of the approximated solution change depending only on the changes of the flux; hence the quantities are conserved. This property is very preferable for problems of conservation laws which are essential in many research fields, e.g., fluid dynamics. secondly, finite volume methods do not use point-wise values but average ones on each control volume, thus unstructured grids can be constructed to adapt with difficult geometries. Based on these reasons, finite volume methods are dominant in computational fluid dynamics and aerodynamics.

3.1 Classical Finite Volume

In this section, we apply finite volume discretizations in approximating the solution of Eq. (1.1.1). For clarification, we rewrite Eq. (1.1.1) as follows:

$$\begin{cases} L_\epsilon := -\epsilon u_{xx} - bu_x = f & \text{in } \Omega = (-1, 1), \\ u(-1) = u(1) = 0, \end{cases} \quad (3.1.1)$$

where $0 < \epsilon \ll 1$, $b = b(x)$, $f = f(x)$ are smooth on $[-1, 1]$, and for $\delta > 0$, $b < 0$, for $-\delta < x < 0$, $b(0) = 0$, $b > 0$ for $0 < x < \delta$, and $b_x(0) > 0$.

Firstly, we define the mesh parameters for our scheme. We rather use a uniform mesh for our computation. Let x_j, u_j be nodal points and values, respectively. The x_j are located at $x = -1 + (j - 1/2)h$, $h = 2/N$, $j = 0, 1, 2, \dots, N, N + 1$ where h is the mesh size and N is the number of control volumes (see Fig. 3-1). The points x_0, x_{N+1} are called ghost points or fictitious points which do not belong to the computational domain Ω and their nodal values u_0, u_{N+1} are determined via boundary conditions and appropriate interpolations at the boundaries (see (3.1.7) and (3.1.8) below). Then the control volumes at x_j have faces at $x_{j-\frac{1}{2}} = x_j - h/2$, $x_{j+\frac{1}{2}} = x_j + h/2$, $j = 1, 2, \dots, N$. Note that the boundary points are $x_{\frac{1}{2}} = -1$, $x_{N+\frac{1}{2}} = 1$.

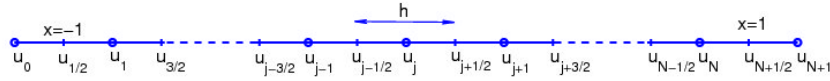


Figure 3-1: Grid system used for the numerical method.

For finite volume methods, we use step functions for discretization purposes. Hence, the solution u and its derivative u_x are interpolated as follows:

$$u \approx u_h = \sum_{j=1}^N u_j \chi_{(x_{j-\frac{1}{2}}, x_{j+\frac{1}{2}})}(x), \quad u_x \approx \nabla_h u_h = \sum_{j=0}^N \frac{u_{j+1} - u_j}{h} \chi_{(x_j, x_{j+1})}(x), \quad (3.1.2)$$

where $u_j = u(x_j)$ and $\chi_{(a,b)}(x)$ is the characteristic function of the interval (a, b) .

In [15], it is proved that

$$\begin{cases} |u - u_h|_{L^2(x_{\frac{1}{2}}, x_{N+\frac{1}{2}})} \leq \kappa h |u|_{H^1(x_{\frac{1}{2}}, x_{N+\frac{1}{2}})}, \\ |u_x - \nabla_h u_h|_{L^2(x_0, x_{N+1})} \leq \kappa h |u|_{H^2(x_0, x_{N+1})}. \end{cases} \quad (3.1.3)$$

Hence, we are motivated to discretize Eq. (3.1.1) via (3.1.2) with the unknown nodal values u_j . The function u_h thus belongs to the finite dimensional space V_h , which is a classical finite

volume space, where

$$V_h = \bigoplus_{j=1}^N \mathbb{R}\phi_j(\cdot), \quad (3.1.4)$$

with

$$\phi_j = \phi_j(x) = \chi_{(x_{j-\frac{1}{2}}, x_{j+\frac{1}{2}})}(x), \quad j = 1, \dots, N. \quad (3.1.5)$$

When we integrate the first derivative over a control volume, i.e.,

$$\int_{x_{j-\frac{1}{2}}}^{x_{j+\frac{1}{2}}} u_x \, dx = u(x_{j+\frac{1}{2}}) - u(x_{j-\frac{1}{2}}), \quad (3.1.6)$$

we need to interpolate these values using the nodal values u_j , $j = 1, \dots, N$ since u_h is not defined at the volume faces $x_{j-\frac{1}{2}}$, $x_{j+\frac{1}{2}}$. Here, we adopt a central difference scheme at faces, including the boundaries:

$$u(-1) = u(x_{\frac{1}{2}}) \approx u_h(x_{\frac{1}{2}}) = \frac{u_0 + u_1}{2} = 0, \quad (3.1.7)$$

$$u(1) = u(x_{N+\frac{1}{2}}) \approx u_h(x_{N+\frac{1}{2}}) = \frac{u_N + u_{N+1}}{2} = 0, \quad (3.1.8)$$

$$u(x_{j+\frac{1}{2}}) \approx u_h(x_{j+\frac{1}{2}}) = \frac{u_j + u_{j+1}}{2}, \quad j = 1, \dots, N-1. \quad (3.1.9)$$

Hence, from (3.1.2), $\nabla_h u_h$ is,

$$\nabla_h u_h = \frac{2u_1}{h} \chi_{[x_{\frac{1}{2}}, x_1)}(x) + \frac{-2u_N}{h} \chi_{(x_N, x_{N+\frac{1}{2}}]}(x) + \sum_{j=1}^{N-1} \frac{u_{j+1} - u_j}{h} \chi_{(x_j, x_{j+1})}(x). \quad (3.1.10)$$

Eq. (3.1.1) is discretized by multiplying by the step functions $\chi_{(x_{j-\frac{1}{2}}, x_{j+\frac{1}{2}})}(x)$ and integrating over Ω , we obtain that

$$-\epsilon u_x \Big|_{x_{j-\frac{1}{2}}}^{x_{j+\frac{1}{2}}} - \int_{x_{j-\frac{1}{2}}}^{x_{j+\frac{1}{2}}} b(x) u_x \, dx = \int_{x_{j-\frac{1}{2}}}^{x_{j+\frac{1}{2}}} f(x) \, dx, \quad j = 1, \dots, N, \quad (3.1.11)$$

which is equivalent to

$$(-\epsilon u_x - b(x)u) \Big|_{x_{j-\frac{1}{2}}}^{x_{j+\frac{1}{2}}} + \int_{x_{j-\frac{1}{2}}}^{x_{j+\frac{1}{2}}} b(x)u \, dx = \int_{x_{j-\frac{1}{2}}}^{x_{j+\frac{1}{2}}} f(x) \, dx, \quad j = 1, \dots, N. \quad (3.1.12)$$

Substituting the approximations (3.1.2) into Eq. (3.1.12), we obtain that

$$(-\epsilon \nabla_h u_h - b(x)u_h + b(x)u_j) \Big|_{x_{j-\frac{1}{2}}}^{x_{j+\frac{1}{2}}} = \int_{x_{j-\frac{1}{2}}}^{x_{j+\frac{1}{2}}} f(x) dx, \quad j = 1, \dots, N. \quad (3.1.13)$$

Applying the boundary conditions (3.1.7), (3.1.8) and arranging terms, we can write the classical finite volume discretization (3.1.13) as follows, for $j = 1, \dots, N$,

$$a_{j,j-1}u_{j-1} + a_{j,j}u_j + a_{j,j+1}u_{j+1} = f_j. \quad (3.1.14)$$

This system corresponds to (3.2.13)–(3.2.14) below with deleting the first row and column.

However, as indicated in the interpolation errors (3.1.3), if $|u|_{H^1}$, $|u|_{H^2}$ are large, e.g., due to the large gradient of u , the numerical approximation will be poor. Indeed, the classical numerical method experiences oscillations (see some numerical examples in section 3 below) near the large gradient of the solution due to the sharp transition layer. To understand why oscillations occur in the numerical solutions of the classical finite volume method, we look at the algebraic system (3.2.13) with Eq. (3.1.14) with $a_{j,j-1}$, $a_{j,j}$ and $a_{j+1,j}$ written as below:

$$a_{j-1,j} = -\frac{\epsilon}{h} + \frac{1}{2}b(x_{j-\frac{1}{2}}), \quad a_{j,j} = -\frac{\epsilon}{h} - \frac{1}{2} \left[b(x_{j+\frac{1}{2}}) - b(x_{j-\frac{1}{2}}) \right], \quad a_{j+1,j} = -\frac{\epsilon}{h} - \frac{1}{2}b(x_{j+\frac{1}{2}}). \quad (3.1.15)$$

As pointed out in [22] (see case 2 of example 5.1, p. 137), in order that the solutions of the algebraic system (3.2.13) are stable, the entries of matrix \mathcal{A} must satisfy the following two conditions:

- the diagonal entries are dominant, i.e.,

$$|a_{jj}| \geq \sum_{j \neq i} |a_{ij}|, \quad \text{for all } j. \quad (3.1.16)$$

- all a_{ij} with $i \neq j$ must have the same sign (all positive or negative).

The first condition is satisfied for our system. But for the second condition, we must have a grid of size

$$h \leq \frac{2\epsilon}{\|b\|_\infty}, \quad (3.1.17)$$

where

$$\|b\|_\infty = \max_{1 \leq j \leq N} |b_j|, \quad (3.1.18)$$

which is impractical in most cases, especially for small ϵ , say, e.g., $\epsilon = 10^{-5}$. To overcome such numerical difficulties, near the sharp layer, we correct the numerical approximation by incorporating appropriate analytic functions which are derived in the following section.

3.2 New Finite Volume

In this section, we present a new approximation method based on Finite Volume to numerically approximate the non-stiff part with the transition layer correctors derived in the previous section. We consider two cases: a single interior transition layer with compatible and noncompatible data.

3.2.1 Compatible Case

Using step functions, we discretize the non-stiff smooth part u_s with finite volumes. From the decomposition (2.3.1) we approximate u by a new trial function \tilde{u}_h ,

$$\begin{cases} \tilde{u}_h = u_h + \lambda\theta^0, \\ u_h = \sum_{j=1}^N u_j \chi_{(x_{j-\frac{1}{2}}, x_{j+\frac{1}{2}})}(x). \end{cases} \quad (3.2.1)$$

Notice that $\tilde{u}_h \approx u$ and $u_h \approx u_s$. As in (2.3.13), boundary conditions for u_h are as follows:

$$\begin{cases} \tilde{u}_h(x_{\frac{1}{2}}) = u_h(x_{\frac{1}{2}}) + \lambda\theta^0(-1) = 0, \\ \tilde{u}_h(x_{N+\frac{1}{2}}) = u_h(x_{N+\frac{1}{2}}) + \lambda\theta^0(1) = 0, \end{cases} \quad (3.2.2)$$

where $x_{\frac{1}{2}} = -1$, $x_{N+\frac{1}{2}} = 1$.

Here the mesh data are adopted from the classical Finite Volume in section 2.1.

The function $\tilde{u}_h \approx u$ thus belongs to the finite dimensional space

$$\tilde{V}_h = V_h \oplus \mathbb{R}\theta^0(\cdot), \quad (3.2.3)$$

where V_h is defined in (3.1.4).

We now discretize Eq. (2.3.12) with (2.3.13). Since θ^0 is asymptotically close to θ , the term $\theta^0 - \theta$ is small and absorbed in other entries in the discrete system (3.2.13)–(3.2.14). Hence, we may drop $\lambda(\theta^0 - \theta)$. If necessary, to achieve higher accuracy, we can introduce a higher asymptotic expansion which replaces θ^0 . Since u_s is slow, as we did in the classical scheme,

using a central difference method at faces including the boundaries, from (3.2.2) we write that

$$u_s(-1) = u_s(x_{\frac{1}{2}}) \approx u_h(x_{\frac{1}{2}}) = \frac{u_0 + u_1}{2} = -\lambda\theta^0(-1), \quad (3.2.4)$$

$$u_s(1) = u_s(x_{N+\frac{1}{2}}) \approx u_h(x_{N+\frac{1}{2}}) = \frac{u_N + u_{N+1}}{2} = -\lambda\theta^0(1), \quad (3.2.5)$$

$$u_s(x_{j+\frac{1}{2}}) \approx u_h(x_{j+\frac{1}{2}}) = \frac{u_j + u_{j+1}}{2}, \quad j = 1, \dots, N-1. \quad (3.2.6)$$

In the same way, we write a new approximation for u_x as follows, for $h = h_j = x_{j+1} - x_j$,

$$\begin{cases} \nabla_h \tilde{u}_h = \nabla_h u_h + \lambda\theta_x^0, \\ \nabla_h u_h = \sum_{j=0}^N \frac{u_{j+1} - u_j}{h} \chi_{(x_j, x_{j+1})}(x). \end{cases} \quad (3.2.7)$$

Notice that $\nabla_h \tilde{u}_h \sim u_x$ and $\nabla_h u_h \sim u_{sx}$. Using the boundary conditions (3.2.4) and (3.2.5), the numerical derivative $\nabla_h u_h$ can be rewritten as:

$$\begin{aligned} \nabla_h u_h &= \frac{2u_1 + 2\lambda\theta^0(-1)}{h} \chi_{[x_{\frac{1}{2}}, x_1)}(x) \\ &+ \frac{-2\lambda\theta^0(1) - 2u_N}{h} \chi_{(x_N, x_{N+\frac{1}{2}}]}(x) + \sum_{j=1}^{N-1} \frac{u_{j+1} - u_j}{h} \chi_{(x_j, x_{j+1})}(x). \end{aligned} \quad (3.2.8)$$

With respect to the unknown λ , we first multiply (2.3.12) by the test function θ^0 and integrate over Ω . However, as a test function, θ^0 is expected to make the stiffness matrix highly ill-conditioned because θ^0 is almost constant except at a small neighborhood of the turning point $x = 0$, and the constants are easily approximated by other test functions, i.e., step functions. Hence, we modify θ^0 to be much distinguished from the linear combination of other test step functions and we thus define the test function ϕ which satisfies zero boundary conditions:

$$\phi = \theta^0 - \theta^0(1)x. \quad (3.2.9)$$

Multiplying (2.3.12) by ϕ and integrating over the domain Ω , after dropping the term $\lambda(\theta^0 - \theta)$, we obtain that

$$\int_{-1}^1 u_{sx}(\epsilon\phi_x - b(x)\phi) = \int_{-1}^1 f(x)\phi, \quad (3.2.10)$$

and using the approximations (3.2.7)–(3.2.8), we find that

$$\begin{aligned} & \frac{2u_1 + 2\lambda\theta^0(-1)}{h}I(-1, -1 + \frac{1}{2}h) + \frac{-2\lambda\theta^0(1) - 2u_N}{h}I(1 - \frac{1}{2}h, 1) \\ & + \sum_{j=1}^{N-1} \frac{u_{j+1} - u_j}{h}I(x_j, x_{j+1}) = \int_{-1}^1 f(x)\phi, \end{aligned} \quad (3.2.11)$$

where $I(a, b) = \int_a^b (\epsilon\phi_x - b(x)\phi)$.

We then obtain the equation as follows:

$$a_{00}\lambda + a_{01}u_1 + a_{0N}u_N + \sum_{j=2}^{N-1} a_{0j}u_j = f_0, \quad (3.2.12)$$

which corresponds to the first row and column of the system (3.2.13) – (3.2.14) below.

From Eq. (2.3.12), dropping the term $\lambda(\theta^0 - \theta)$, we then derive the same discretized equation as (3.1.13) with u_h , ∇u_h of the conventional scheme replaced by the new approximations \tilde{u}_h , $\nabla_h \tilde{u}_h$ as in Eqs. (3.2.1) and (3.2.7). Then using the boundary conditions (3.2.4)–(3.2.6), we can similarly obtain the same system as Eq. (3.1.14). Combining with the additional Eq. (3.2.12), we obtain a discrete system which incorporates the corrector θ^0 :

$$\mathcal{A}\mathbf{u} = \mathbf{f}, \quad (3.2.13)$$

where $\mathcal{A} = \mathcal{A}_\epsilon = (a_{ij}^\epsilon)$, $\mathbf{u} = (\lambda, u_1, \dots, u_N)^T$, $\mathbf{f} = (f_0, f_1, \dots, f_N)^T$, and for $i, j = 0, \dots, N$, $l = 2, \dots, N-1$, $m = 1, \dots, N$.

$$\left\{ \begin{array}{l}
 a_{00} = \frac{2}{h} \left[\theta^0(-1)I(-1, -1 + \frac{1}{2}h) - \theta^0(1)I(1 - \frac{1}{2}h, 1) \right], \\
 a_{01} = \frac{1}{h} \left[2I(-1, -1 + \frac{1}{2}h) - I(-1 + \frac{1}{2}h, -1 + \frac{3}{2}h) \right], \\
 a_{0l} = \frac{1}{h} \left[I(-1 + (l - \frac{3}{2})h, -1 + (l - \frac{1}{2})h) - I(-1 + (l - \frac{1}{2})h, -1 + (l + \frac{1}{2})h) \right], \\
 a_{0N} = \frac{1}{h} \left[-2I(1 - \frac{1}{2}h, 1) + I(1 - \frac{3}{2}h, 1 - \frac{1}{2}h) \right], \\
 a_{10} = \left[\frac{2\epsilon}{h} - b(-1) \right] \theta^0(-1), \\
 a_{11} = \frac{3\epsilon}{h} + \frac{1}{2}b(x_{\frac{3}{2}}) - b(-1), \\
 a_{12} = -\frac{\epsilon}{h} - \frac{1}{2}b(x_{\frac{3}{2}}), \\
 a_{l,l-1} = -\frac{\epsilon}{h} + \frac{1}{2}b(x_{l-\frac{1}{2}}), \\
 a_{l,l} = \frac{2\epsilon}{h} + \frac{1}{2} \left[b(x_{l+\frac{1}{2}}) - b(x_{l-\frac{1}{2}}) \right], \\
 a_{l,l+1} = -\frac{\epsilon}{h} - \frac{1}{2}b(x_{l+\frac{1}{2}}), \\
 a_{N0} = \left[\frac{2\epsilon}{h} + b(1) \right] \theta^0(1), \\
 a_{N,N-1} = -\frac{\epsilon}{h} + \frac{1}{2}b(x_{N-\frac{1}{2}}), \\
 a_{N,N} = \frac{3\epsilon}{h} - \frac{1}{2}b(x_{N-\frac{1}{2}}) + b(1), \\
 f_0 = \int_{-1}^1 f(x)\phi, \\
 f_m = \int_{x_{m-\frac{1}{2}}}^{x_{m+\frac{1}{2}}} f(x),
 \end{array} \right. \tag{3.2.14}$$

and all other entries vanish. Here, we recall $I(a, b) = \int_a^b (\epsilon\phi_x - b(x)\phi)$. Notice that the system (3.2.13)–(3.2.14) is tridiagonal, except for the first row, and can be solved easily by using the sparsity of \mathcal{A} .

3.2.2 Noncompatible Case

In this section, we present a numerical approximation scheme for the solution of Eq. (3.1.1) where $b(x)$ and $f(x)$ are noncompatible, i.e., when $f(0) \neq 0 = b(0)$.

We, therefore, introduce a new decomposition for the approximation of the solution of (3.1.1) as follows:

$$u = u_s + \lambda\theta^0 + f(0)\varphi^0. \tag{3.2.15}$$

Table 3-1: Comparison on L^2 and L^∞ errors of the classical FVM (cFVM) and the new FVM (nFVM) using the corrector θ^0 with the exact solution (4.1.2) of Eq. (4.1.1) with different values of ϵ and numbers of control volumes N .

ϵ	N	cFVM		nFVM	
		L^2 error	L^∞ error	L^2 error	L^∞ error
10^{-1}	40	1.200E-03	1.800E-03	9.429E-04	1.700E-03
10^{-1}	80	3.029E-04	4.695E-04	2.362E-04	4.413E-04
10^{-1}	160	7.573E-05	1.189E-04	5.904E-05	1.123E-04
10^{-1}	320	1.893E-05	2.990E-05	1.477E-05	2.828E-05
10^{-2}	40	1.600E-03	2.300E-03	1.800E-03	2.600E-03
10^{-2}	80	3.820E-04	5.617E-04	4.543E-04	6.555E-04
10^{-2}	160	9.476E-05	1.372E-04	1.135E-04	1.633E-04
10^{-2}	320	2.365E-05	3.439E-05	2.838E-05	4.883E-05
10^{-3}	40	1.650E-02	4.240E-02	2.600E-03	6.700E-03
10^{-3}	80	2.400E-03	8.800E-03	5.637E-04	1.400E-03
10^{-3}	160	5.560E-04	2.000E-03	1.392E-04	3.310E-04
10^{-3}	320	1.366E-04	4.982E-04	4.470E-05	8.400E-05
10^{-4}	40	3.150E-02	8.630E-02	2.200E-03	4.200E-03
10^{-4}	80	2.390E-02	6.940E-02	1.100E-03	3.400E-03
10^{-4}	160	4.500E-03	2.280E-02	1.907E-04	8.462E-04
10^{-4}	320	8.474E-04	5.300E-03	4.192E-05	1.961E-04
10^{-5}	40	4.900E-03	1.330E-02	1.800E-03	2.400E-03
10^{-5}	80	1.100E-02	4.240E-02	4.817E-04	9.954E-04
10^{-5}	160	1.840E-02	9.540E-02	2.975E-04	1.300E-03
10^{-5}	320	9.200E-03	6.300E-02	1.063E-04	7.367E-04

Substituting (3.2.15) into Eq. (3.1.1) and using (2.3.5), (2.3.10), we obtain that

$$L_\epsilon(u_s + \lambda(\theta^0 - \theta) + f(0)(\varphi^0 - \varphi)) = f(x) - f(0), \text{ in } \Omega. \quad (3.2.16)$$

Since θ^0 , φ^0 are asymptotically close to θ , φ , respectively, similarly we may drop the terms $\lambda(\theta^0 - \theta)$, $f(0)(\varphi^0 - \varphi)$. Higher order asymptotic terms which replace θ^0 , φ^0 can be adapted for higher accurate schemes, if necessary.

The right-hand side $f(x) - f(0)$ is compatible with $b(x)$ at $x = 0$, and the logarithmic singularity is analytically resolved.

Eq. (3.2.16) is supplemented with boundary conditions:

$$\begin{cases} u_s(-1) + \lambda\theta^0(-1) + f(0)\varphi^0(-1) = u(-1) = 0, \\ u_s(1) + \lambda\theta^0(1) + f(0)\varphi^0(1) = u(1) = 0. \end{cases} \quad (3.2.17)$$

Applying the new method to (3.2.16) and dropping the terms $\lambda(\theta^0 - \theta)$, $f(0)(\varphi^0 - \varphi)$, we obtain the system (3.2.13)–(3.2.14) with the following modification in \mathbf{f} , due to the boundary

Table 3-2: Comparison on L^2 and L^∞ errors of the cFVM and the nFVM with the exact solution (4.1.2) of Eq. (4.1.1), $N = 160$.

ϵ	cFVM		nFVM	
	L^2 error	L^∞ error	L^2 error	L^∞ error
10^{-1}	7.573E-05	1.189E-04	5.904E-05	1.123E-04
10^{-2}	9.476E-05	1.372E-04	1.135E-04	1.633E-04
10^{-3}	5.560E-04	2.000E-03	1.392E-04	3.310E-04
10^{-4}	4.500E-03	<i>2.280E-02</i>	1.907E-04	8.462E-04
10^{-5}	1.840E-02	<i>9.540E-02</i>	2.975E-04	1.300E-03
10^{-6}	3.300E-03	<i>1.750E-02</i>	1.158E-04	2.332E-04

conditions (3.2.17):

$$\left\{ \begin{array}{l} f_0 = -\frac{2}{h} \left[I(-1, -1 + \frac{1}{2}h)f(0)\varphi^0(-1) - I(1 - \frac{1}{2}h, 1)f(0)\varphi^0(1) \right] + \int_{-1}^1 (f(x) - f(0))\phi, \\ f_1 = -\left(\frac{2\epsilon}{h} - b(-1)\right) f(0)\varphi^0(-1) + \int_{x_{\frac{1}{2}}}^{x_{\frac{3}{2}}} (f(x) - f(0)), \\ f_N = -\left(\frac{2\epsilon}{h} + b(1)\right) f(0)\varphi^0(1) + \int_{x_{N-\frac{1}{2}}}^{x_{N+\frac{1}{2}}} (f(x) - f(0)), \\ f_m = \int_{x_{m-\frac{1}{2}}}^{x_{m+\frac{1}{2}}} (f(x) - f(0)), \quad m = 2, \dots, N-1. \end{array} \right. \quad (3.2.18)$$

Remark 3.2.1. For both compatible and noncompatible cases, we use the same discretizations u_h and $\nabla_h u_h$ to approximate u_s and u_{sx} , respectively. The former is the same for both cases as well as for the classical scheme, but the latter is different due to the boundary conditions as in (3.1.7), (3.1.8) for the classical scheme, (3.2.2) for the compatible case, and (3.2.17) for the noncompatible case.

IV

Results and Discussions

In this section, we present a number of examples to illustrate the accuracy and efficiency of our new method.

4.1 Compatible Case

We first consider the compatible case where condition $b(0) = 0 = f(0)$ is satisfied. We rewrite Eq. (3.1.1) with the right-hand side $f(x)$ specified as below:

$$\begin{cases} -\epsilon u_{xx} - xu_x = f(x) = 3\operatorname{erf}\left(\frac{1}{\sqrt{2\epsilon}}\right)(x^3 + 2\epsilon x), \\ u(-1) = u(1) = 0. \end{cases} \quad (4.1.1)$$

An exact solution is available for Eq. (4.1.1), which is as follows:

$$u_e = \operatorname{erf}\left(\frac{x}{\sqrt{2\epsilon}}\right) - \operatorname{erf}\left(\frac{1}{\sqrt{2\epsilon}}\right)x^3. \quad (4.1.2)$$

We approximate the solution of Eq. (4.1.1) with the classical and new FVM schemes (cFVM, nFVM). For the nFVM, the corrector $\lambda\theta^0$ with the zeroth term θ^0 as in (2.3.7) is used in the simulation. We notice that only the non-stiff part u_s as in (2.3.1) is approximated by solving the system (3.2.13)–(3.2.14). The numerical solution \tilde{u}_h , is then constructed by using the decomposition (3.2.1).

Results for both schemes are plotted, together with the exact solution (4.1.2), in Fig. 4-1 with $\epsilon = 10^{-4}$ and mesh size $h = 2/N = 2/40$. As indicated in the interpolation errors (3.1.3), with such a coarse mesh, the cFVM exhibits oscillations near the turning point (see also Figs. 4-6 and 4-8); whereas the nFVM well captures the sharp transition layer. We recall that the transition layer of the nFVM is an analytical solution, captured by the corrector $\lambda\theta^0$ where θ^0 is the zeroth term of the asymptotic expansion as in (2.3.6)–(2.3.5). Furthermore, meshes used

for the transition layer of the new method are *uniform and independent* of the small parameter ϵ . We notice that in case of the cFVM scheme, exponentially refined meshes are required near the transition layer. Hence, the former is *much more efficient than* the latter scheme.

Numerical errors, measured in L^2 and L^∞ norms, of the two schemes are estimated and listed in Table 3-1, with a variety in values of ϵ and mesh sizes h , and in Table 3-2, with a fixed mesh size $h = 2/N = 2/160$. It is shown that the nFVM shows much better accuracy for small values of ϵ and both cFVM and nFVM schemes have the same order of accuracy for $\epsilon \geq 10^{-2}$. Furthermore, as indicated in Table 2, the nFVM is *very robust* with respect to changes in ϵ , whereas the cFVM loses accuracies as ϵ tends to be small.

Since the cFVM cannot capture the singularity of the transition layer, the errors caused by oscillations near them contaminate the accuracy of the whole computational domain Ω . Hence, the nFVM is *more stable* and, in general, *more accurate than* cFVM. This conclusion is depicted in Fig. 4-2 where numerical errors of both schemes are plotted with $\epsilon = 10^{-4}$ and different mesh sizes h . For Figs. 4-2 and 4-3–4-4 discussed below, we plot the errors in log scale vs. n where $N = 2^n \times 10$ is the number of control volumes.

In Figs. 4-3 and 4-4, L^2 and L^∞ errors of the new scheme are plotted with different values of ϵ and mesh sizes h . From the figures, we draw two conclusions. Firstly, 2^{nd} -ordered convergence is achieved for the new method. Secondly, there are differences between the errors of the outer and inner solutions, which are most clearly seen in L^∞ errors (see Fig. 4-4) where the plots depend on ϵ linearly in log scales. This is due to asymptotic errors because in the inner expansion, only the zeroth term θ^0 (see (2.3.6), (2.3.5), and (2.3.7)) is used as the corrector in the decomposition (2.3.1). The asymptotically small term $\lambda(\theta^0 - \theta)$ in (2.3.12) is dropped and considered absorbed by other entries in the system (3.2.13)–(3.2.14). It can be also seen in Table 3-1. In case of $\epsilon = 10^{-5}$, there is an increase in the L^∞ errors for the nFVM when the mesh is refined from $N = 160$ to $N = 320$. From the observance in the remark 2.2.2, we assert that this discrepancy can be reduced if more asymptotic terms are introduced in the corrector, in case higher order of accuracy is required.

In Fig. 4-5, different right-hand side functions $f(x)$ are simulated to illustrate the robustness of the new method for the compatible case.

4.2 Non-compatible Case

In this section, examples for the noncompatible case are given. We first consider the following problem:

$$\begin{cases} -\epsilon u_{xx} - xu_x = f(x) = \cos\left(\frac{\pi}{2}x\right) + x, \\ u(-1) = u(1) = 0. \end{cases} \quad (4.2.1)$$

Here, $b(0) = 0$ and $f(0) = 1$. Hence, $b(x)$ and $f(x)$ are noncompatible. We apply the decomposition (3.2.15) with adding the zeroth corrector φ^0 , the boundary conditions as in (3.2.17). The system (3.2.13)–(3.2.14) are then solved with \mathbf{f} modified as in (3.2.18). Numerical solutions from the cFVM and nFVM are shown in Fig. 4-6. As in the compatible case, the nFVM scheme well resolves the asymptotic and logarithmic singularity and there are oscillations in case of the cFVM scheme in both outer and inner regions. The oscillations are much stronger than those in the compatible case. However, the nFVM scheme is very robust and captures the large gradient near the transition layer for both compatible and noncompatible cases.

In Fig. 4-7, more examples are given to illustrate for the noncompatible case with $b(x) = x$ and different $f(x)$'s on the right-hand side of Eq. (4.2.1). It can be seen that logarithmic singularity is very well resolved.

The last example is tested for the case when $b(x) = \sin x$ with $f(x) = x$ and $f(x) = 1$ for a compatible and noncompatible case, respectively. We notice that the same correctors, θ^0 as in (2.3.7) and φ^0 as in (2.3.8), are applied in this simulation because only the zeroth terms, which approximate (2.3.5) and (2.3.10), respectively, are used as the correctors. Results are plotted in Fig. 4-8 for the compatible case, Fig. 4-9 for the noncompatible case.

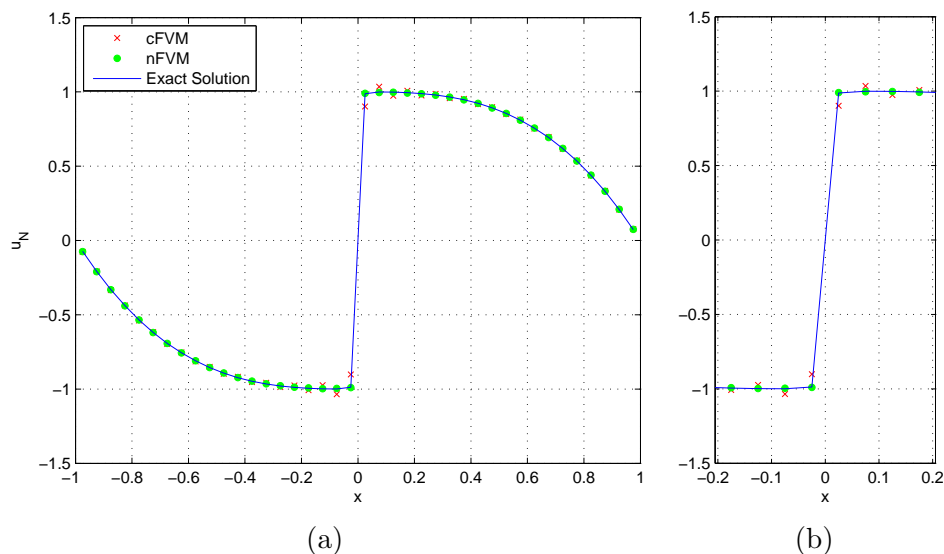


Figure 4-1: (a) Numerical solutions u_N of Eq. (4.1.1) from the classical FVM (cFVM) vs. new FVM (nFVM) using corrector θ^0 : $\epsilon = 10^{-4}$, $N = 40$; (b) Zooming near the transition layer.

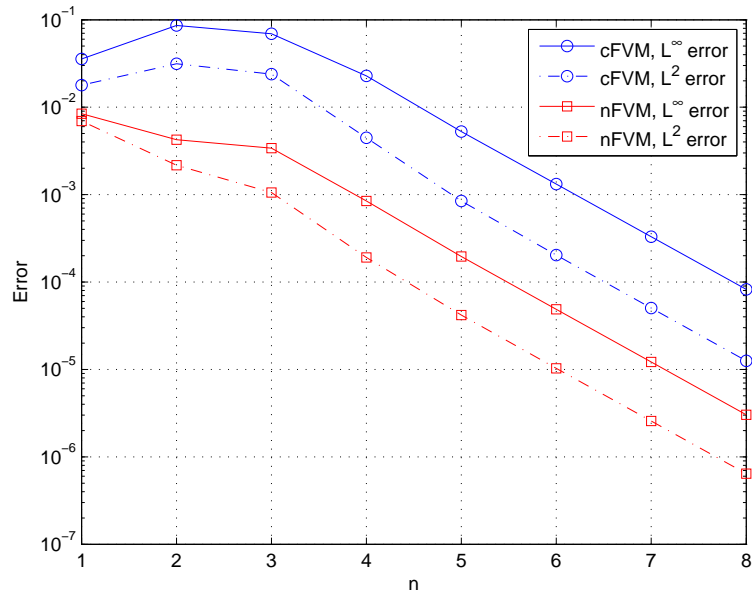


Figure 4-2: Error plotting of numerical solutions of Eq. (4.1.1) from the cFVM vs. nFVM: $\epsilon = 10^{-4}$, $N = 2^n \times 10$ is the number of control volumes.

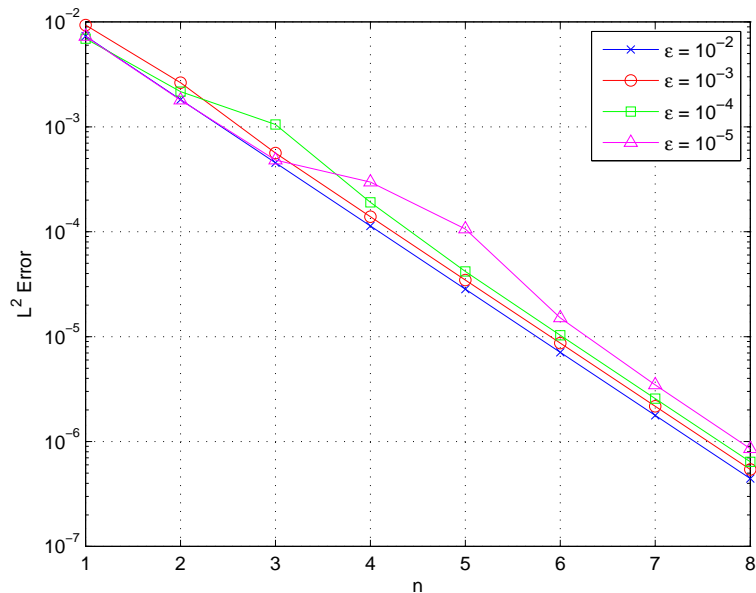


Figure 4-3: L^2 error plotting of numerical solutions of Eq. (4.1.1) from the nFVM with different values of ϵ , $N = 2^n \times 10$ is the number of control volumes.

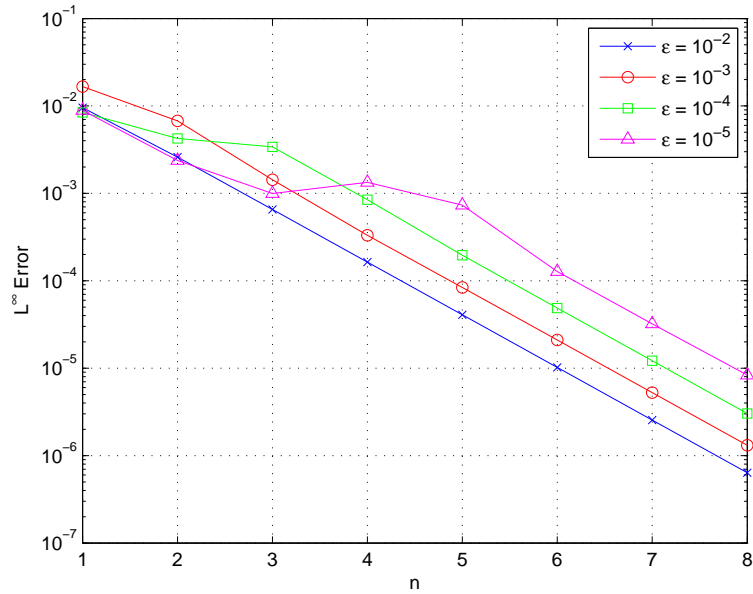


Figure 4-4: L^∞ error plotting of numerical solutions of Eq. (4.1.1) from the nFVM with different values of ϵ , $N = 2^n \times 10$ is the number of control volumes.

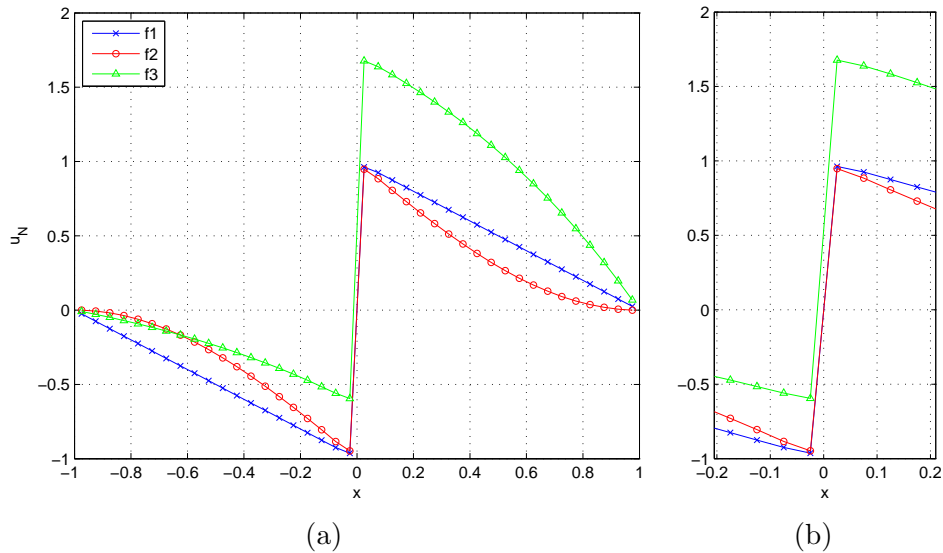


Figure 4-5: (a) Numerical solutions u_N from nFVM with $b(x) = x$ and $f(x) = f_j(x)$ for the compatible case: $f_1(x) = x$, $f_2(x) = -\frac{\pi}{2} \operatorname{erf}\left(\frac{1}{\sqrt{2\epsilon}}\right) \left[\frac{\pi}{2} \epsilon \sin\left(\frac{\pi}{2}x\right) - x \cos\left(\frac{\pi}{2}x\right)\right]$, $f_3(x) = xe^x$, $\epsilon = 10^{-4}$, $N = 40$; (b) Zooming near the transition layer.

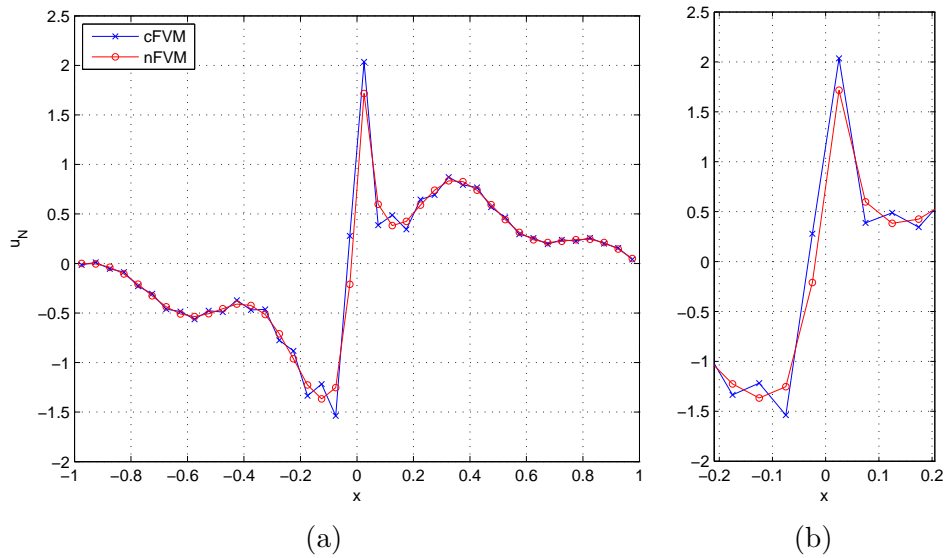


Figure 4-6: (a) Numerical solutions u_N of Eq. (4.2.1) from the cFVM vs. nFVM using two correctors θ^0 and φ^0 : $\epsilon = 10^{-4}$, $N = 40$ for the noncompatible case; (b) Zooming near the transition layer.

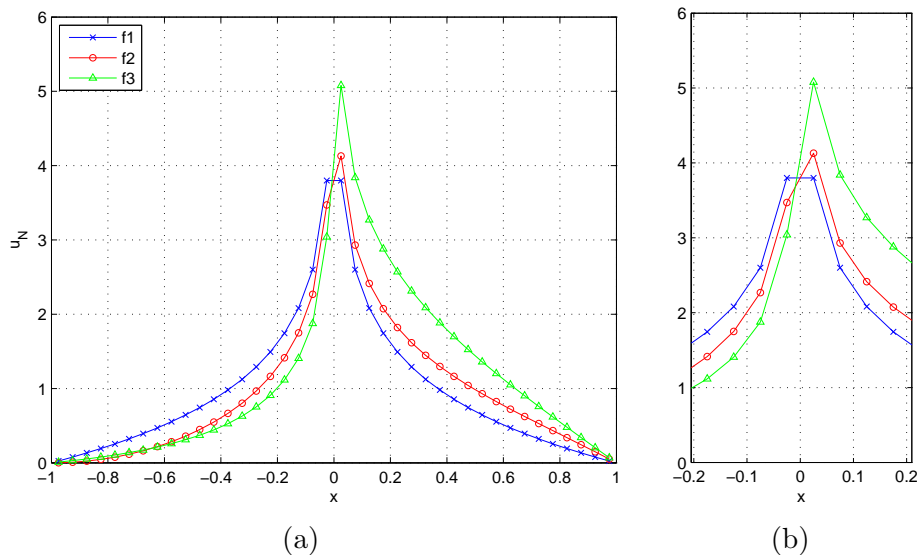


Figure 4-7: (a) Numerical solutions u_N from nFVM with $b(x) = x$ and $f(x) = f_j(x)$ for the noncompatible case: $f_1(x) = 1$, $f_2(x) = x^3 + 1$, $f_3(x) = e^x$, $\epsilon = 10^{-4}$, $N = 40$; (b) Zooming near the transition layer.

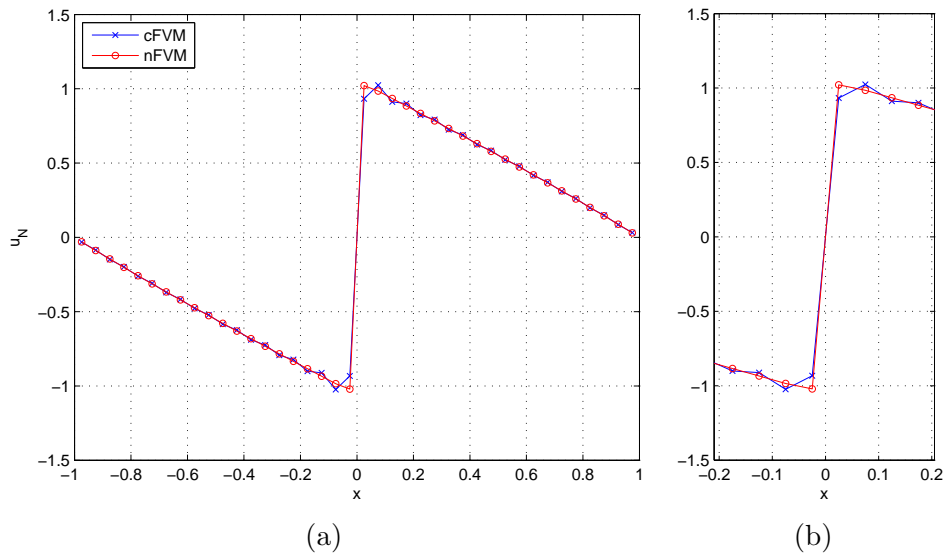


Figure 4-8: (a) Numerical solutions u_N from cFVM vs. nFVM with $b(x) = \sin x$, $f(x) = x$, $\epsilon = 10^{-4}$, $N = 40$ for the compatible case; (b) Zooming near the transition layer.

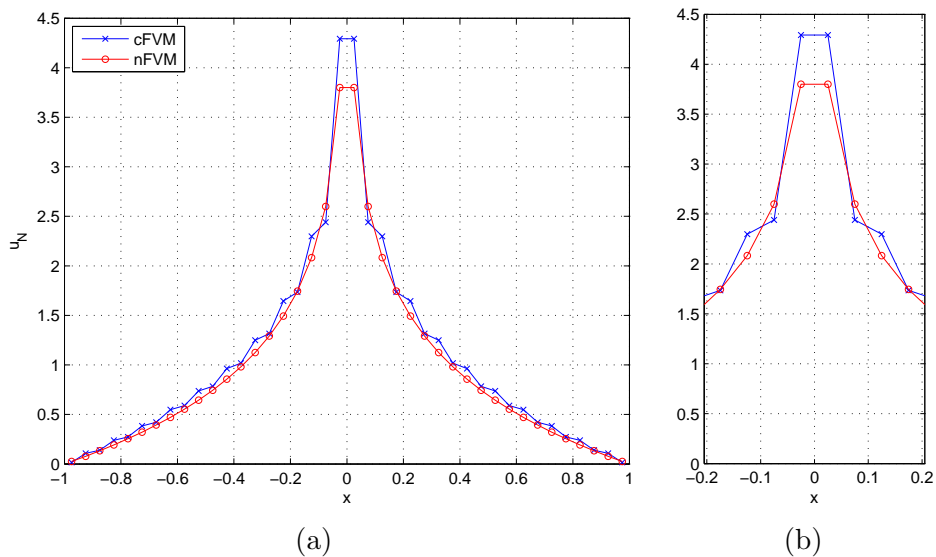


Figure 4-9: (a) Numerical solutions u_N from cFVM vs. nFVM with $b(x) = \sin x$, $f(x) = 1$, $\epsilon = 10^{-4}$, $N = 40$ for the noncompatible case; (b) Zooming near the transition layer.

V

Conclusion

In this work, we have proposed a new numerical method based on finite volume approach to approximate stiff problems having an interior transition layer near a turning point $x = x_0$. Firstly, the analytical solution θ for the transition layer is derived by employing singular perturbation analysis. It turned out that only the zeroth term θ^0 is enough for numerical purposes. However, in higher order schemes, more asymptotic terms as in (2.3.2) will be needed. This layer, incorporating with an unknown λ , is added to enrich the classical finite volume space.

The problem has been also studied in a more complicated case with the occurrence of logarithmic singularity near the turning point due to the noncompatibility in the data of the problem. One more corrector φ as in (2.3.10) is added into the solution decomposition as in (3.2.15) so that the problem can be transformed into a compatible case analytically. Hence, the new scheme can now be applied; new boundary conditions (3.2.17) are then imposed, and thus the right-hand side \mathbf{f} is modified as in (3.2.18).

A variety of examples are given to illustrate the accuracy, stability and efficiency of the new method in section 3 with different coefficients $b(x)$ and right-hand side functions $f(x)$, both for compatible and noncompatible cases.

The technique presented in this article can be further developed for more complex cases. If we have multiple transition layers at $x = x_j$, introducing a Lagrange interpolating polynomial, we write:

$$P_j(x) = \prod_{\substack{k=1 \\ k \neq j}}^n \frac{x - x_k}{x_j - x_k}, \quad f(x) = \sum_{l=1}^n P_l(x) f(x). \quad (5.0.1)$$

Here, we used the fact that $Q(x) := \sum_{l=1}^n P_l(x) = 1$ because $Q(x_j) = 1$, $j = 1, 2, \dots, n$ and $Q(x)$ is of degree $n - 1$. Then $P_j(x)f(x) = 0$ at $x = x_l$, $l = 1, 2, \dots, n$, $l \neq j$, but $P_j(x)f(x)$ may not be compatible at $x = x_j$, i.e., $P_j(x_j)f(x_j) = f(x_j) \neq 0$. For this single noncompatible point x_j , we have already treated in the text.

Writing the solution of Eq. (1.1.1) $u = \sum_{j=1}^n v^j$ where

$$L_\epsilon(v^j) = P_j(x)f(x), \quad v^j = 0 \text{ at } x = \pm 1, \quad (5.0.2)$$

and applying the numerical techniques in the text to each equation (5.0.2), thanks to the superposition of the solutions, we finally obtain the numerical solution u_N for u . Parallel computing in this case is well suited because Eq. (5.0.2) can be solved independently at each processor j , $j = 1, 2, \dots, n$.

Combining with the previous results (see e.g. [15]), boundary layer correctors can be also incorporated, and if the coefficient $b(x)$ has zeros at $x = x_j$ with multiplicity, the form of the correctors should be changed according to the singular perturbation analysis at $x = x_j$. All these changes can be adapted without difficulties. For instance, if $b(x) = (x - 1/2)(x + 1/2)$ in the model (1.1.1), there are a boundary layer at the outflow $x = -1$ and a transition layer at the turning point $x = 1/2$. Or in multi-dimensional problems, the derivative in the convective term is replaced by the gradient of $u(x)$. These issues will be discussed elsewhere.

References

- [1] Andronov, I, Bouche D & Molinet, F 2005, *Asymptotic and hybrid methods in electromagnetics*, IEE Electromagnetic Waves Series 48. [2](#)
- [2] Batchelor, GK 1988, *An Introduction to Fluid Dynamics*, Cambridge University Press, Cambridge. [2](#)
- [3] Cheng, W & Temam, R 2002, 'Numerical approximation of one-dimensional stationary diffusion equations with boundary layers', *Comput. Fluids* **31**, pp. 453-466. [7](#), [8](#)
- [4] Cheng, W, Temam, R & Wang, X 2000, 'New approximation algorithms for a class of partial differential equations displaying boundary layer behavior', *Methods Appl. Anal.* **7**, pp. 363-390.
- [5] Desanti, AJ 1987, 'Nonmonotone interior layer theory for some singularly perturbed quasi-linear boundary value problems with turning points', *SIAM J. Math. Anal.* **18**, pp. 321-331. [5](#)
- [6] Drazin, PG & Reid, WH 2004, *Hydrodynamic Stability, 2nd edn*, Cambridge University Press, Cambridge.
- [7] Eckhaus, W 1972, 'Boundary layers in linear elliptic singular perturbations', *SIAM Rev.* **14**, pp. 225-270. [5](#)
- [8] Eckhaus, W & de Jager, EM 1966, 'Asymptotic solutions of singular perturbation problems for linear differential equations of elliptic type', *Arch. Rational Mech. Anal.* **23**, pp. 26-86.
- [9] Holmes, MH 1995, *Introduction to Perturbation Methods*, Springer, New York. [5](#), [12](#)
- [10] Han, H & Kellogg, RB 1982, *A method of enriched subspaces for the numerical solution of a parabolic singular perturbation problem.* in *Computational and Asymptotic Methods for Boundary and Interior Layers*, Dublin, pp. 46-52. [5](#)
- [11] Johnson, RS 2005, *Singular Perturbation Theory*, Springer Science+Business Media, Inc., New York. [5](#), [11](#), [20](#)

-
- [12] Jung, C & Temam, R 2005, ‘Numerical approximation of two-dimensional convection-diffusion equations with multiple boundary layers’, *Internat. J. Numer. Anal. Model.* **2**, pp. 367-408. [7](#), [8](#)
- [13] Jung, C & Temam, R 2007, ‘Asymptotic analysis for singularly perturbed convection-diffusion equations with a turning point’, *J. Mathematical Physics*, **48**, 065301. [5](#), [8](#), [9](#), [15](#), [19](#), [20](#), [21](#)
- [14] Jung, C 2008, ‘Finite elements scheme in enriched subspaces for singularly perturbed reaction-diffusion problems on a square domain’, *Asymptot. Anal.* **57**, pp. 41-69. [8](#)
- [15] Jung, C & Temam, R 2009, ‘Finite volume approximation of one-dimensional stiff convection-diffusion equations’, *J. Sci. Comput.* **41**, no. 3, pp 384-410. [7](#), [8](#), [25](#), [42](#)
- [16] Kellogg, RB & Stynes, M 2008, ‘Layers and corner singularities in singularly perturbed elliptic problems’, *BIT* **48**(2), pp. 309-314. [5](#)
- [17] O’Malley, RE 2008, ‘Singularly perturbed linear two-point boundary value problems’, *SIAM Rev.* **50**, no. 3, pp 459-482. [5](#)
- [18] Stynes, M 2005, ‘Steady-state convection-diffusion problems’, *Acta Numer.*, **14**, pp. 445-508. [6](#), [7](#)
- [19] Shih, S & Kellogg, RB 1987, ‘Asymptotic analysis of a singular perturbation problem’, *Siam J. Math. Anal.* **18**, pp . 1467-1511. [5](#)
- [20] Temam, R & Wang, X 2002, ‘Boundary layers associated with incompressible Navier-Stokes equations: the noncharacteristic boundary case’, *J. Differential Equations*, **179**, no. 2, pp. 647-686.
- [21] Vishik, MI & Lyusternik, LA 1957, ‘Regular degeneration and boundary layer for linear differential equations with small parameter’, *Usp. Mat. Nauk* **12**, 3.122.
- [22] Versteeg, HK & Malalasekera, W 2007, *An Introduction to Computational Fluid Dynamics: The Finite Volume Method, 2nd ed.*, Pearson/Prentice Hall. [6](#), [24](#), [27](#)
- [23] Wasow, W 1985, *Linear Turning point Theory*, Springer, New York. [5](#)
- [24] Kalashnikova, I, Tezaur, R & Farhat, C 2010, ‘A Discontinuous Enrichment Method for Variable Coefficient Advection-Diffusion at High Peclet Number’, *Int. J. Numer. Meth. Engng.* **87**, pp. 309-335. [8](#)
- [25] LeVeque, RJ, *Finite volume methods for hyperbolic problems*, Cambridge University Press, Cambridge, 2004. [24](#)

- [26] LeVeque, RJ, *Numerical methods for conservation laws*, Birkhäuser Verlag, Basel, Switzerland, 2004. [2](#), [7](#)
- [27] Smith, DR, *Singular perturbation theory*, Cambridge University Press, New York, 1985. [5](#)
- [28] Roos, HG, Stynes, M, & Tobiska, L, *Robust numerical methods for singularly perturbed differential equations: Convection-diffusion-reaction and flow problems*, Springer-Verlag, Berlin, Heidelberg, 2008. [6](#), [7](#)

ACKNOWLEDGEMENTS

Firstly, I would like to express my sincere gratitude to my advisor, Professor Chang-Yeol Jung for accepting me as his student. I would have never completed the Master's program and this thesis without his extensive and constant guidance and support. I own him my deepest thanks for his prompt answers to whatever questions I have.

I would like to express my appreciation to Professor Chun Sang Yoo, and Professor Pilwon Kim for their advice and suggestions during the preparation of this thesis.

I would also like to give thanks to my labmates and friends for their generous helps, both in study and in life.

Finally, I would like to thank my family, especially my parents, for their encouragement, love and care for me on every step of my life.

